Analytica Chimica Acta 1202 (2022) 338894

Contents lists available at ScienceDirect

Analytica Chimica Acta

journal homepage: www.elsevier.com/locate/aca

Review

Quartz-enhanced photoacoustic spectroscopy for multi-gas detection: A review

Angelo Sampaolo [a, b], Pietro Patimisco [a, b], Marilena Giglio [a, b], Andrea Zifarelli [a, b], Hongpeng Wu [a], Lei Dong [a, **], Vincenzo Spagnolo [a, b, *]

[a] State Key Laboratory of Quantum Optics and Quantum Optics Devices, Institute of Laser Spectroscopy & Collaborative Innovation Center of Extreme Optics, Shanxi University, Taiyuan, 030006, China
[b] Polysense Lab, Dipartimento Interateneo di Fisica, University and Politecnico of Bari, CNR-IFN, Via Amendola 173, Bari, 70126, Italy

HIGHLIGHTS

- Quartz-Enhanced Photoacoustics for for multi-gas laser spectroscopy.
- Trace gas detection of non-interfering absorbers.
- Isotopic ratio measurements.
- Trace gas detection of broadband absorbers.
- Analysis of complex gas mixtures and fluctuating backgrounds.

GRAPHICAL ABSTRACT

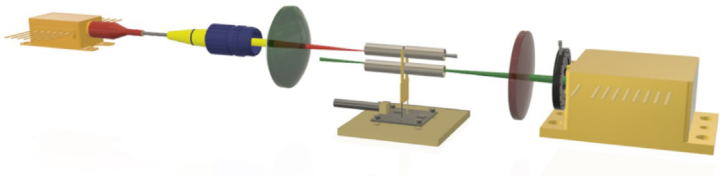

ARTICLE INFO

Article history:
Received 7 April 2021
Received in revised form
2 July 2021
Accepted 26 July 2021
Available online 2 August 2021

Keywords:
Gas sensing
Quartz-enhanced photoacoustic spectroscopy
Multi-gas detection
Broadband absorbers

ABSTRACT

Multi-gas detection represents a suitable solution in many applications, such as environmental and atmospheric monitoring, chemical reaction and industrial process control, safety and security, oil&gas and biomedicine. Among optical techniques, Quartz-Enhanced Photoacoustic Spectroscopy (QEPAS) has been demonstrated to be a leading-edge technology for addressing multi-gas detection, thanks to the modularity, ruggedness, portability and real time operation of the QEPAS sensors. The detection module consists in a spectrophone, mounted in a vacuum-tight cell and detecting sound waves generated via photoacoustic excitation within the gas sample. As a result, the sound detection is wavelength-independent and the volume of the absorption cell is basically determined by the spectrophone dimensions, typically in the order of few cubic centimeters. In this review paper, the implementation of the QEPAS technique for multi-gas detection will be discussed for three main areas of applications: i) multi-gas trace sensing by exploiting non-interfering absorption features; ii) multi-gas detection dealing with overlapping absorption bands; iii) multi-gas detection in fluctuating backgrounds. The fundamental role of the analysis and statistical tools will be also discussed in detail in relation with the specific applications. This overview on QEPAS technique, highlighting merits and drawbacks, aims at providing ready-to-use guidelines for multi-gas detection in a wide range of applications and operating conditions.

* Corresponding author. State Key Laboratory of Quantum Optics and Quantum Optics Devices, Institute of Laser Spectroscopy & Collaborative Innovation Center of Extreme Optics, Shanxi University, Taiyuan, 030006, China.
** Corresponding author.
E-mail addresses: donglei@sxu.edu.cn (L. Dong), vincenzoluigi.spagnolo@poliba.it (V. Spagnolo).

https://doi.org/10.1016/j.aca.2021.338894

Contents

1. Introduction: Motivations and applications for multi-gas laser spectroscopy

The possibility to perform multi-gas detection over a wide concentration range is crucial for many gas sensing application fields. Environmental monitoring, safety and security, oil&gas and biomedical applications demand for real time and in-situ solutions together with unambiguous identification and quantification of the chemical analytes composing the investigated gas samples. Gas spectroscopy exploiting laser sources is a reliable tool providing highly selective and sensitive detection by means of robust and compact sensor architectures. The mid-infrared spectral region is particularly suitable for spectroscopy of broadband absorbers and strongly overlapping gas species, like NOx, CO, CO_2 and hydrocarbons. In the petroleum exploration field, the concentration and the isotope ratio of the alkanes and of other non-hydrocarbon components reveal the origin of the natural gas and help in estimating the reserves [1]. For biomedical applications, the fast response characterizing optical techniques enables an on-line analysis of the patients' breath and detection of one, or potentially several, tumor markers at the same time [2]. The possibility to detect different gas species by employing one only sensor finds a huge amount of applications, spanning from environmental monitoring (greenhouse gases) to industrial process control (toxic and dangerous gases), from life science research to biomedical and pharmaceutical applications (human breath sensing) [3–7]. Nowadays, infrared multi-gas detection systems are the subject of study and investigations in many research institutes and companies: Rice University (U.S.), Aereodyne Inc (U.S.), Los Gatos Research, MQ Photon Research Center (AUS), North University (CHN), Anhui Institute of Optics and Fine Mechanics (CHN), Pranalytica Company (CA), Polysense Lab (IT), just to name a few. The very basic element for a spectroscopic sensor is the light source, which can be first classified as coherent or non-coherent (Fig. 1).

The infrared non-coherent light sources employed so far in gas sensing mostly consist in light emitting diodes (LEDs). Infrared LEDs have a wavelength emission range from 0.83 to 12 μm, optical powers higher than 100 mW at room temperature or even lower and modulation bandwidths as high as 100 MHz [8]. The coherent light sources can be divided into two major groups: near and mid-infrared lasers. All near-infrared laser technologies share common spectral features, namely narrow linewidths (<1 MHz) and emission wavelengths tuning up to tens of nanometers. These devices can also provide approximately single-frequency operation with optical powers in the order of tens of mW. Their extensive employment in the telecommunication field makes these devices reliable, robust and extremely versatile in terms of implementation into spectroscopic setups and sensor architectures, because of their pigtailed single-mode fibers that make the beam delivery very easy and efficient [9].

The mid-IR lasers market suitable for spectroscopic applications is dominated by the interband cascade lasers (ICLs) and the quantum cascade lasers (QCLs). These two laser technologies mainly differ in wavelength tunability, power consumption, linewidth and optical power. The intrinsic linewidth, the typical wavelength tunability range and optical power for a distributed feedback ICL (DFB-ICL) are in the order of tens of kHz, tens of nm and tens of mW, respectively. The room temperature operation usually does not require an active cooling system and the power consumption is typically <1 W [10]. For distributed feedback QCLs (DFB-QCL),

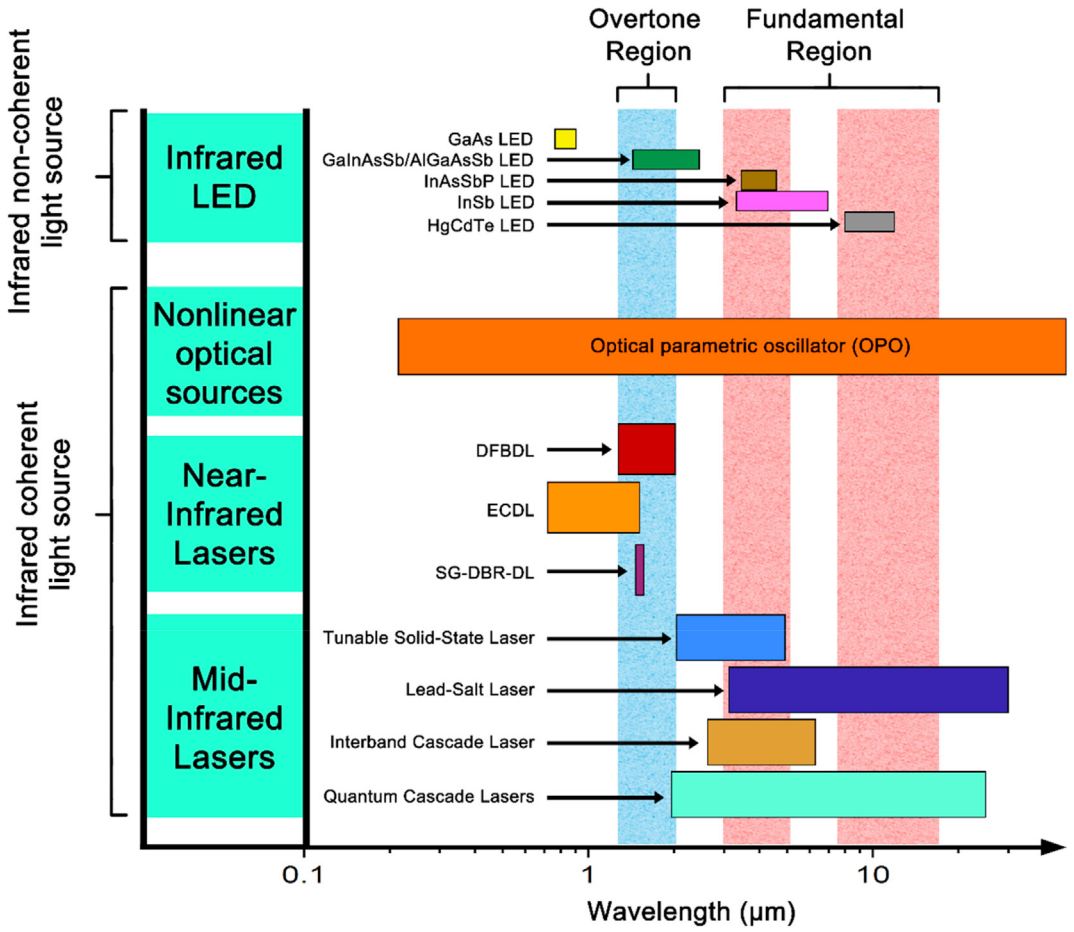

Fig. 1. Light sources with related wavelength emission range.

average values would be hundreds of kHz of intrinsic linewidth, tens of nm of wavelength tunability range and up to the watt scale of optical power. In most cases, QCLs require an active air or water cooling to cope with a heat dissipation requirement compatible with power consumptions in the order of few watt [11]. Configurations in which single laser devices are coupled with external cavities can extend tunability ranges in the order of microns [12].

The infrared non-coherent light sources emit continuous wavelength spectra in a wide range, thus, in principle, these devices are intrinsically devoted to multi-gas and broadband detection. However, the radiation power density is relatively low and wavelength selectors, like optical filters, must be used when a selective excitation of a specific absorbing species is needed. All these limiting factors affect irretrievably the selectivity and sensitivity of the sensors, reducing the detection limits at the part-per-million (ppm) scale in the best case scenario. Although such a detection level can be good enough for some industrial or agricultural applications, high power laser sources with narrow spectral emission must be necessarily employed to enhance the detection sensitivity. By employing these laser sources, trace gas detection sensitivities in the part-per-billion (ppb) concentration scale are typically achieved. Nevertheless, the high cost and power consumption of devices like ICLs or QCLs must be always taken into account when designing a laser-based sensor system.

Once identified the laser source suitable for the multi-gas detection required by a specific application, the spectroscopic method must be chosen, with the consequent identification of the other core element of optical gas sensors: the detector. In all direct absorption techniques, the Beer–Lambert's law puts in relation the light absorption with the gas properties. If P_0 is the optical power incident on the gas sample, the attenuated optical power P transmitted through the sample is:

$$P = P_0 e^{-\alpha l} \tag{1}$$

where α is the absorption coefficient of the gas sample and l is the optical pathlength. The absorption coefficient is defined as the product between the absorption cross section, proportional to the linestrength of the radiative transition, and the number of molecules per unit volume, proportional to the target gas concentration. Considering that the highest detection sensitivity is most desirable, the minimum detection limit (MDL) is one of the most important figures of merit identified for all gas sensors, defined as the target gas concentration giving a signal equal to the 1σ standard deviation of the noise level. The normalized noise equivalent absorption (NNEA) defined as the minimum absorption coefficient (calculated by using MDL) normalized to the optical power and the signal integration time, is also considered to compare the performances of different optical sensors [13,14]. For each analyte, the straightforward approach to improve the MDL is to choose, if possible, the strongest line of the fundamental absorption band of the target gas and exploit a fairly high optical pathlength [4]. Multi-pass absorption cells are commonly used in spectroscopy to improve detection sensitivity by increasing the total optical pathlength, hopefully keeping the light-gas interaction volume as small as possible. The laser beam is reflected back and forth at the surfaces

of two large concave mirrors, creating a reflection pattern confined within the volume of the absorption cell. Once the laser beam exits the cell, an optical detector is placed close to the exit hole to sense laser power attenuation due to its interaction with the absorbing analyte in the gas mixture under investigation. Large optical pathlengths require precise alignments to preserve the pattern of laser beam reflections between the two mirrors. Nevertheless, multi-pass cells are commercially available and have been successfully employed in several optical sensors over the last years [15,16]. Another way to increase the interaction between the laser radiation and the absorbing gas species is to use high-finesse cavities as optical resonators (cavity-enhanced absorption spectroscopy, CEAS). In the simplest configuration, the optical cavity is composed of two high reflectivity (>99.9%) mirrors arranged in order to form a Fabry–Perot etalon. Thus, an optical cavity is much more sensitive to optical misalignments with respect to a multi-pass cell. In addition, a high spatial quality laser beam as well as a narrow spectral linewidth are strict requirements for reaching high sensing performances [17]. It is worth noting that both optical cavities and multi-pass cells are usually designed for a specific operation wavelength, therefore their performance dramatically deteriorates when coupled with broadband sources, precluding their use for multi-gas detection [18].

Among indirect optical absorption techniques, photoacoustic spectroscopy (PAS) plays a central role. PAS detects weak sound waves generated by the photoacoustic excitation occurring within an absorbing gas. Thus, PAS does not require an optical detector; moreover a sound detector is wavelength insensitive [19]. When the laser optical power is modulated at a certain frequency, the molecules experience a sequence of absorption/release of the accumulated optical energy, resulting in a modulation of molecules' spatial density. Nonradiative collisional processes transfer this energy to neighborhood molecules, giving rise to pressure waves, i.e., sound, propagating far from the absorption region. The easiest way to detect sound wave is to place a sensitive microphone in the cell containing the absorbing gas. Moreover, the geometry of the cell is designed in order to amplify the sound waves, properly generated at a frequency resonant with the fundamental acoustic mode of the cell, typically in the range 1–4 kHz [19]. The main parameter characterizing the resonance mode is the quality factor *Q*, defined as 2π times the ratio of the stored energy to the energy dissipated per oscillation cycle. It can be also defined via the resonance bandwidth, as the ratio of the resonance frequency ν_0 to the full width at half-maximum (FWHM) bandwidth $\delta\nu$ of the resonance, $Q = \nu_0/\delta\nu$. For a resonance mode of an acoustic cell, the quality factor is tipically lower than 200.

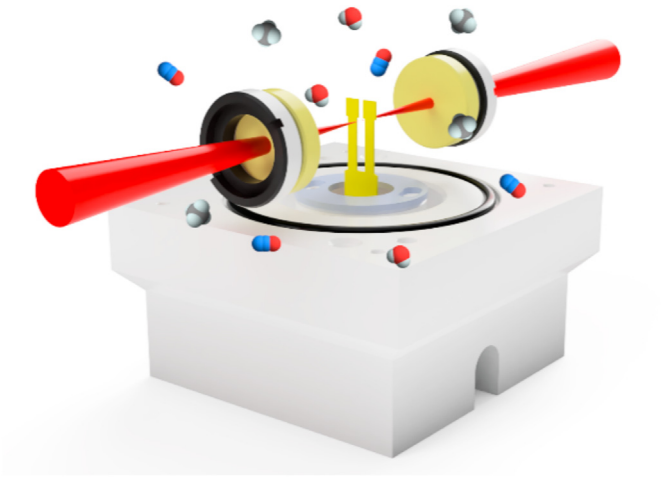

Fig. 2. Schematic of a photoacoustic excitation in a QEPAS apparatus.

In the perspective of removing restrictions imposed by the size of the acoustic cell and employing mechanical resonators with quality factors >10,000, quartz enhanced photoacoustic spectroscopy (QEPAS) was subsequently developed, using quartz tuning forks (QTF) to sense the sound waves within a narrow frequency bandwidth [20]. This spectroscopic technique is intrinsically devoted to i) out-of-laboratory applications, because of the unmatchable ruggedness and compactness of the sensors, and ii) multi-gas detection, because of the wavelength independence of the sensitive element operation. Furthermore, the QTF is an acoustic quadrupole, providing a good environmental noise immunity. On the other hand, the gas matrix influence on sound generation and QEPAS detection sets some undeniable boundaries to the application of this technique [13,14].

In this review all the merits and weaknesses of the QEPAS approach for multi-gas detection will be discussed through a systematic classification of the most representative multi-gas QEPAS sensors and configurations demonstrated in literature up to date.

2. Quartz enhanced photoacoustic spectroscopy

2.1. Basic principles

Starting from 2002, QTFs have been widely used as sound detectors in photoacoustic spectroscopy [20]. In QEPAS, a modulated light source is focused between QTF prongs and sound waves are generated via photoacoustic effect, as schematically depicted in Fig. 2. The very basic principle of operation for employing a QTF as a sound detector requires the laser modulation frequency to be set at one of the QTF resonance frequencies, which are related to different prong motions, such as in- and out-of-plane flexural modes, bending, twisting, symmetric and anti-symmetric. As better discussed in paragraph 2.5, the first in-plane anti-symmetric flexural mode is usually referred as the fundamental vibrational mode, while the third in-plane anti-symmetric flexural mode is more conveniently called first overtone mode. Thus, when the acoustic wave puts both prongs in their natural oscillation motion, a stress field along the prong is generated. In other words, the laser beam can be treated as a cylindrical acoustic source, inducing prong vibrations due to the pressure wavefronts hitting the prong internal surface. In the elastic regime, the stress field induces a strain field which in turn generates a local polarization of the quartz. As a consequence, charges appear on the surface that can be collected by electrical contacts properly deposited along the QTF prong. The strain field as well as piezoelectric charge distribution are mainly localized at the prong clamped-end.

Once collected a piezoelectric signal, this can be demodulated at the same laser modulation frequency, which is resonant with a specific vibrational mode of the QTF or at one of its higher harmonics, as it will be explained more in detail in the next paragraph. The resonance properties of a QTF suitable for QEPAS must satisfy two conditions: i) a resonance frequencies <40 kHz, since the nonradiative collisions among molecules occur on a microsecond time scale [13,14]; ii) low gas damping losses while the QTF vibrates, which means a high quality factor. The first QTF employed in a QEPAS sensor was a standard tuning fork normally used for timekeeping in watches and smartphones, with a resonance frequency of ~32.78 kHz and a quality factor >13,000 at atmospheric pressure and room temperature [13,14,20]. From 2013, custom QTFs have been designed and optimized for QEPAS operation with a resonance frequency spanning from 3 to 40 kHz, and quality factors >10,000 at atmospheric pressure. One way to excite a flexural mode is to generate the sound wave between QTF's prongs, so that the

prongs will vibrate in-phase, in two opposite directions (anti-symmetric flexural mode). Phenomenologically, the QEPAS signal can be supposed proportional to:

$$S \sim Q \cdot P \cdot \alpha \cdot \varepsilon \tag{2}$$

where ε is the radiation-to-sound conversion efficiency, which is dependent on nonradiative collisional rate and expresses the capability of gas to convert the absorbed optical power in sound wave generation. Thus, the performance of QEPAS-based sensors depends on: i) the employed laser output power; ii) the characteristics of the target absorbing molecule, such as the optical transition excited and the related oscillator strength; iii) QTF's resonance frequency compared to the relaxation rate of the target molecule within a specific gas matrix [14].

2.2. Modulation/demodulation approaches for signal processing

A narrow spectral linewidth, together with a high optical power and a fast tunability of a diode laser source set the basis for reaching very high detection sensitivities when modulation techniques are adopted [4]. Amplitude modulation (AM) is obtained for example by placing a rotating chopper wheel right after the laser output to periodically block the light and generate a square-wave modulated power. Wavelength modulation (WM) is typically pursued by applying a sinusoidal modulation to the laser current to generate both a modulation of the laser power and of the wavelength, at the same frequency. For both AM and WM approaches, the acquired signal (i.e., the QTF signal in QEPAS) must be demodulated at the modulation frequency or at higher harmonics. In this way, the influence of the *1/f* noise, the direct current offset, and the evenly distributed random noise are suppressed, resulting in an improved signal-to-noise ratio (SNR). Two approaches are widely used for demodulating the signal: digital lock-in detection and Fourier transform [21].

2.2.1. Derivative spectroscopy: photoacoustic generation by wavelength modulation

When the laser diode current is sinusoidally dithered, both its wavelength and laser power are modulated, as a consequence of the linear dependence of the wavelength and of the laser power on the injected current above the lasing threshold. Thus, a modulation of the laser current at a frequency ω, $i(t) = i_0 + \Delta i \cdot \cos(\omega t)$, generates a modulation of the optical power $P(t) = P_0 + \Delta P \cdot \cos(\omega t)$ and of the instantaneous laser frequency $\nu(t) = \upsilon_0 + \Delta\nu \cdot \cos(\omega t + \psi)$. Assuming $\Delta\nu << \upsilon_0$, the absorption coefficient $\alpha[\upsilon(t)]$ can be expanded as a Taylor series around υ_0. By combining the Taylor expansion with the Beer–Lambert's law (see Eq. (1)), the transmitted power for a weakly absorbing gas becomes [21,22]:

$$P(t) = [P_0 + \Delta P \cos(\omega t)] \times \left[1 - \alpha(\upsilon_0) l - \alpha'(\upsilon_0)\Delta\upsilon \cos(\omega t) l - \frac{1}{2}\alpha''(\upsilon_0)\Delta\upsilon^2 \cos^2(\omega t) l\right] \tag{3}$$

However, $\cos^2(\omega t)$ terms will be proportional to 1/2 [1 + cos(2ωt)]. If the laser current is modulated at ω and the lock-in demodulates the generated signal at the same frequency (WM and 1ω-detection), the resulting signal will be:

$$S_{1\omega} = \Delta P \cos(\omega t) - \Delta P \alpha(\upsilon_0) l \cos(\omega t) - P_0 \alpha'(\upsilon_0)\Delta\upsilon \cos(\omega t) l \tag{4}$$

By linearly varying the injected current i(t), both the emission frequency and the laser output power are assumed to linearly vary as well. As a consequence, the spectral scan across the Lorentzian-like gas absorption line will resemble the first-derivative of a Lorentzian function (the third term of Eq. (4)) with a flat background (the first and second terms). Conversely, if the laser current is modulated at ω and the lock-in demodulates the generated signal at the double frequency (WM and *2ω*-detection), the resulting demodulated signal $S_{2\omega}$ will be:

$$S_{2\omega} = -\Delta P \alpha'(\upsilon_0)\Delta\upsilon \cos(\omega t)\cos(\omega t) l + \frac{1}{4} P_0 \alpha''(\upsilon_0)\Delta\upsilon^2 \cos(2\omega t) l \tag{5}$$

$S_{2\omega}$ consists in two terms, the first proportional to the first-derivative and the second one containing the second-derivative of the Lorentzian function. Thus, a spectral scan across the gas absorption line will results in a background-free, second-derivative of a Lorentzian lineshape function distorted by the first-derivative term, the latter proportional to the amplitude of the power modulation ΔP (residual amplitude modulation). Being the first derivative zero at υ_0, the peak position of $S_{2\omega}$ coincides with the peak position of the real absorption lineshape (supposed to be Lorentzian).

2.2.2. Photoacoustic generation by amplitude modulation

In the case of on–off modulation of the light beam, odd harmonics appear in the signal spectrum, depending on the rise and decay times of the light power during the switching. In the case of slow rise and decay, i.e., ~ from 5% to 10% of the modulation period T_{mod}, the spectrum resembles that of a sinusoidal intensity modulation (AM) and it contains few odd harmonics of the modulation frequency. In the case of a fast rise and decay time (as for a periodic pulse train), the spectrum consists of several odd harmonics of the modulation frequency. However, in the case of fast switching, the portion of the total sound pressure that contributes to the fundamental harmonic is small and, as a result, most of the signal is lost for the photoacoustic measurement [22]. This represents the main difference between the most often-applied modulation methods in photoacoustics: amplitude modulation of a continuous wave (CW) laser and periodic pulse trains of a pulsed laser. In particular, demonstrating that periodic pulse trains are quite ineffective in generating a PAS signal at the repetition frequency. In fact, for typical modulation frequencies compatible with QTF resonance modes, the strongest lines of the spectrum for a pulse train can be observed far beyond 100 kHz, depending on the duration of the primary sound wave and on laser beam size [22]. On the contrary, AM provides a strong fundamental component and a few weak harmonics, given also that a pure sinusoidal photoacoustic signal cannot be achieved because of nonlinear dependence of the light power on the modulation signal [21]. In any case, all the AM spectroscopic approaches may suffer from background absorption not necessarily related with the target molecules.

2.3. Energy relaxation dynamics in gas mixtures

As reported in Eq. (2), the photoacoustic signal depends on the light-to-sound conversion efficiency ε, which quantifies the capability of a gas to generate sound waves as a consequence of the absorbed optical power. When molecules absorb infrared light, roto-vibrational energy states are excited. If the optical absorption is abruptly interrupted, nonradiative processes dominate the release of energy within the gas sample, causing a local heating nearby the volume where the absorption takes place. In addition, collisional processes transfer the absorbed energy from the excited volume to neighbored molecules, and sound waves are then generated (V-T relaxation) [23]. When the optical absorption is intensity-modulated, the modulation frequency must be compared

with the rapidity of gas to completely release the excess of absorbed energy (relaxation rate of the analytes). In other words, if the modulation frequency is too high, the molecules could not follow the fast modulation, causing a partial release of energy for each oscillation period. This results in a low-efficient sound wave generation (slow-relaxing gases) [24–26]. Conversely, fast-relaxing molecules are characterized by relaxation rates faster than the modulation frequency, resulting in a complete release of energy in the gas sample and, in turn, in an efficient sound waves generation [27]. The 32.7 kHz fundamental mode frequency of a standard QTF is usually classified as a high modulation frequency, thus not optimal for slow relaxing gases. Since the sound waves generation involves collisional processes with neighbored molecules, it is straightforward that the composition of gaseous matrix mainly determines the light-to-sound conversion efficiency ε. Therefore, to enhance ε when slow-relaxing gases are excited, fast-relaxing gases (such as H_2O) are usually added to the gas matrix composition at concentrations of few percent. In this case, the fast-relaxing gas acts as a relaxation promoter for the slow-relaxing gas because it enhance the sound wave generation efficiency [28]. For such mixtures, the effective relaxation rate k is empirically calculated as the sum of the absolute relaxation rates k_i of each analyte composing the mixture by using the following expression [29]:

$$k = \sum_i k_i C_i \tag{6}$$

where is C_i is the concentration of the *i-th* analytes.

The influence of the light-to-sound conversion efficiency on photoacoustic signal generation was first studied in 1996 by Repond and Sigrist [30], and then investigated by Wysocki in 2006 [31], by using a QEPAS sensor with a standard 32.7 kHz-QTF for CO_2 detection. In the latter, the CO_2 QEPAS signal was studied at different water vapor concentrations, allowing a measure of the CO_2 absolute relaxation rate. Recently, Dello Russo et al. [29] demonstrated that an accurate estimation of relaxation rates requires an investigation of the light-to-sound conversion efficiency at different modulation frequencies. With this aim, they employed different QTFs with resonance frequencies spanning from 3 kHz to 45 kHz to measure the effective relaxation times of CH_4 and H_2O, obtaining 3.2 ms·Torr and 0.25 ms·Torr, respectively [29].

2.4. Quartz tuning forks

In QEPAS, the optical absorption is mainly localized between prongs, where the acoustic wave is generated. In order to confine and enhance the sound wave, two resonator tubes are usually located on both sides of the QTF [13]. The QTF and micro-resonator tubes constitute the spectrophone, the sensitive element of a QEPAS sensor. The standard QTF is characterized by a prong spacing of 300 μm. When assembled in a spectrophone, a pair of resonator tubes having a length of 4 mm and diameter of 600 μm per each is employed. The laser beam must be properly focused between prongs, while passing through the tubes without hitting them. If modulated light touches the QTF prongs and/or internal wall of tubes, a photo-induced thermal is generated, resulting in a background optical noise [32]. Thus, QTFs with prongs' gap larger than 300 μm can make the optical alignment easier and reduce the optical noise. This requirement, together with the necessity to operate at frequencies lower than 32.7 kHz, paved the way to the realization of custom QTFs optimized for QEPAS sensing [33,34]. The realization of QTFs with prongs gap as large as 1.5 mm allowed the use of light sources with poor spatial beam quality as well as the use of THz laser sources [32]. In addition, a large prong spacing can easily accommodate a single resonator tube, directly placed between QTF prongs, with two lateral slits for exiting the sound wave. When the QTF fundamental mode is lower than ~5 kHz, also the first overtone mode becomes suitable for QEPAS sensing [35,36]. The exploitation of the first overtone mode gave rise to novel QEPAS configurations, such the double-antinode excitation [37] and detection of two different gas species at the same time thanks to the simultaneous excitation of both the fundamental and the first overtone mode [38]. Finally, two novel prong shapes were also proposed: hammer-shaped prongs to reduce the resonance frequency without affecting the quality factor of the resonance [24,39] and rectangular grooves carved on the prong surface to increase the coupling between piezoelectric charges and the resonance mode [40,41].

2.5. Tuning fork vibrational modes and QEPAS configurations

The sizes of a QTF prong can be related with the flexural mode frequencies f_n by using the Euler-Bernoulli theory, which considers each prong as a vibrating rectangular beam, and by imposing the clamped-free boundary conditions to the prong ends' motion [42]:

$$f_n = \frac{\pi T}{8\sqrt{12}L^2}\sqrt{\frac{E}{\rho}}m_n^2 \tag{7}$$

$E = 0.72 \cdot 10^{11}$ N/m^2 and $\rho = 2650$ kg/m^3 are the Young's modulus and the density of quartz, respectively; T and L are the prong length and thickness, respectively; $m_0 = 1.194$ and $m_1 = 2.998$ identify the fundamental ($n = 0$) and the first overtone ($n = 1$) mode, respectively. The Euler-Bernoulli theory predicts also the vibration profile along the y-axis in terms of the distance from the prong base x [43]:

$$y(x) = A\left\{\cosh(k_n x) - \cos(k_n x) + \left[\frac{\sin(k_n L) - \sinh(k_n L)}{\cos(k_n L) + \cosh(k_n L)}\right] \times [\sinh(k_n x) - \sin(k_n x)]\right\} \tag{8}$$

where A is the vibration amplitude and k_n are the wavenumbers related to the eigenfrequencies f_n. Each flexural mode exhibits a vibration profile with n+1 antinode points. In Fig. 3, the vibration profile for the fundamental and first overtone mode is simulated for $L = 17$ mm by using Eq. (8) [44].

The frequency modulation for photoacoustic sensing should be chosen depending on the characteristics and requirements for a specific application in terms of gas target, gas matrix composition, operating pressure, and many other factors. Thus, the suitable custom resonator can be identified by evaluating its resonance frequencies (fundamental or 1st overtone mode) with related quality factors and antinode points of vibration. Several configurations can be adopted to i) increase the interaction pathlength between the laser light and the target molecules between the QTF prongs, such as In-plane QEPAS and Multi-pass QEPAS [45,46]; ii) enhance the pressure wave through amplification systems based on resonator tubes that can be applied to the bare QTF [13,14,24,32]; iii) simultaneously excite different vibrational modes in the same QTF [38].

The next two paragraphs will be focusing the discussion on acoustic resonators for sound wave amplification and on fundamental/overtone mode combined vibration, respectively.

2.5.1. On-beam QEPAS and off-beam QEPAS

Acoustic resonators (ARs) are acoustically coupled with a QTF to form a QEPAS spectrophone. To date, off- and on-beam spectrophone configurations have been realized [13,14]. In the on-beam spectrophone configuration, a QTF is inserted between two

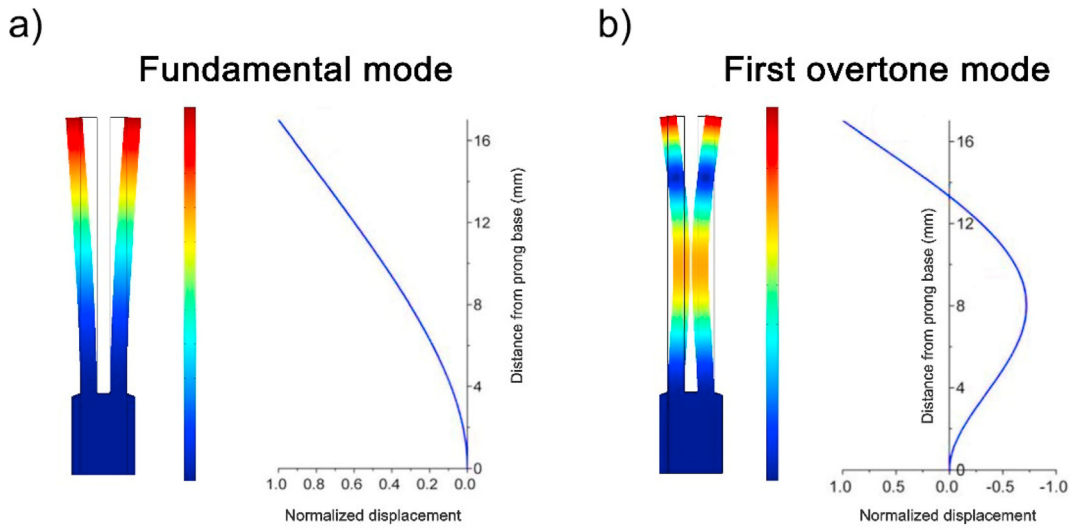

Fig. 3. (a) Vibration profile of the QTF prong having a length of 17 mm for (a) the fundamental and for (b) the first overtone mode. Color bars are used to visualize the displacement on the QTF sketch. The displacement profiles were simulated using COMSOL Multiphysics. (For interpretation of the references to colour in this figure legend, the reader is referred to the Web version of this article.)

cylindrical tubes. In this way, the two tubes act as open-end resonators and the QTF probes the acoustic wave. It is worth noting that the node point of a pressure standing wave created within an open-end resonator lays slightly outside the resonator end. The distance between the resonator end and the node point is referred as the open-end correction which is proportional to the tube radius. Resonance frequencies of an open−end resonator are thus estimated by considering an effective resonator length given by the sum of the resonator length and the open-end correction. Therefore, the effective resonator length must match an integer multiple of half-wavelength of sound [47]. The 4 mm-long tubes applied in correspondence of the fundamental mode antinode of the standard 32 kHz QTF, provide a signal-to-noise (SNR) enhancement factor of ~30. The lower the fundamental resonance frequency, the longer are ARs. The longest tubes thus far implemented in a custom spectrophone, were 23 mm long and mounted with a 7.2 kHz QTF operated at its fundamental mode. The SNR gain obtained was ~40 [48]. Many others ARs were implemented in custom spectrophones, but the largest value of SNR enhancement was demonstrated for a pair of tubes 12.4 mm long, each applied to a T-shaped 12.7 kHz QTF and providing a SNR enhancement of ~60 [24]. These improved values of SNRs are also due to a lower interaction between the laser light and the QTF's structure because of the larger prong spacing of the custom designs. This determines a reduced photo-induced thermal contribution to the noise level.

AR tubes were also applied to the lower antinode of a QTF overtone mode, as demonstrated for example by Giglio et al. with a QTF operating at the first overtone mode with a resonance frequency of 25.4 kHz [49].

A further evolution of on-beam configuration was demonstrated by Zheng et al. and it consists in a single-tube resonator, called SO-QEPAS [50]. In this configuration, the large prong gap of custom QTFs is exploited to accommodate a one-piece tube in the middle, aligned with one antinode of the vibrational mode selected. This tube shows two small slits on both sides at its middle point, from which the spherical acoustic wave propagates towards the inner surface of the prongs. Therefore, the standing wave arising within the 1-D resonator is only minimally deformed on its peak and the resulting acoustic pressure on the QTF is higher with respect to the double-tube configuration.

The SO-QEPAS has the main advantages of increasing the SNR and reducing the tube length closer to the acoustic wavelength. The single tube was tested and implemented both at fundamental and overtone modes, in particular a SNR enhancement of ~128 was measured for a 7.2 kHz QTF at the fundamental mode [50] and a SNR enhancement of ~380 was measured for a 2.8 kHz QTF operated at its first overtone (17.7 kHz) [51]. Both SNR enhancements were calculated with respect to the QEPAS signal obtained for the bare QTFs operated at the fundamental mode.

Another possible configuration where a 1D-resonator tube is employed to create a standing acoustic wave is the off-beam QEPAS. Taking into account the open-end correction, the tube length is determined as for the on-beam spectrophone configuration. However, in this case the tube i) has only one slit in the middle, ii) is positioned parallel to the QTF plane and nearby the prongs and iii) the vertical position of the tube is chosen so that the slit is aligned with one of the vibrational antinodes. K. Liu et al. presented an extensive study of the optimization of geometrical parameters to retrieve the highest SNR for a standard QTF excited in off-beam configuration [52]. In this experiment, both the optimal slit width and length were experimentally found, allowing an enhancement of the QEPAS signal by a factor of ~16 with respect to the bare QTF.

In conclusion, the SNR enhancement with respect to a bare standard QTF of the optimum on-beam configuration has been demonstrated to be almost twice the SNR in the off-beam configuration. The main benefit of the off-beam configuration is that the laser beam does not pass between the QTF prongs. This avoids the photo-induced thermal contribution to the ground noise, which is characteristic, however small, of the on-beam configuration. Thus, the off-beam approach would be intrinsically suited for accommodating high power laser beams as well as poor spatial quality beams. Nevertheless, custom designs of on-beam and off-beam spectrophones [53] have relaxed the constrains on laser sources' characteristics and emission wavelength, allowing the employment of optical powers > 1W [48] as well as THz radiation [32].

2.5.2. Fundamental and overtone combined vibration for simultaneous dual gas detection

In paragraph 2.5, the Euler-Bernoulli theory for modeling a QTF as two single cantilevers characterized by negligible coupling has

been introduced. By imposing the clamped-free boundary conditions, a full set of eigenfrequencies representing linearly independent vibrational modes, can be determined.

Thus, exploiting the non-interfering vibration of different in-plane flexural modes, a QEPAS sensor for simultaneous detection of two gas species was demonstrated and developed by Wu et al. [38]. This was realized by simultaneously exciting the antinode point of the fundamental mode and the lowest antinode point of the first overtone mode (see Fig. 3), with two different laser sources. Therefore, two different analytes can be detected by demodulating the QEPAS signal at two frequencies, namely that of the fundamental mode and of the first overtone mode, as shown in Fig. 4.

The custom QTF employed by Wu at al. for the first dual gas QEPAS demonstration was a 2.8 kHz custom QTF with the overtone frequency at 17.7 kHz. The position of the fundamental and overtone lower antinodes were found respectively ~2 mm and ~9.5 mm below the prong top. This distance allows the simultaneous accommodation of two laser beams for dual-gas detection of H_2O and C_2H_2 [38]. The detection sensitivities for this QEPAS configuration were improved by implementing ARs at both antinodes [54,55] and a single tube at the lower antinode of the overtone [56]. The applications in multi-gas sensing for this approach will be deeply discussed in Chapter 5 where its employment for real-time compensation of target gas signals with respect to the concentration of relaxation promoters, like water, will be illustrated.

3. Trace gas detection of non-interfering absorbers

The trace gas spectroscopy for molecules characterized by optical transitions with a Lorentzian profile is the most suitable condition for QEPAS detection. A multi-gas spectroscopy based on a straight-forward detection scheme and relatively simple analysis of the QEPAS spectra is still possible, as long as the absorption features are well separated and the overall concentration of the target molecules in the matrix is in the order of few per thousand in volume or less. In this paragraph, the experimental conditions enabling an independent detection of different analytes, without taking into account the effects of the matrix variations, will be illustrated and discussed. The QEPAS multi-gas sensors that have been conceived and operated under these conditions will be also reviewed.

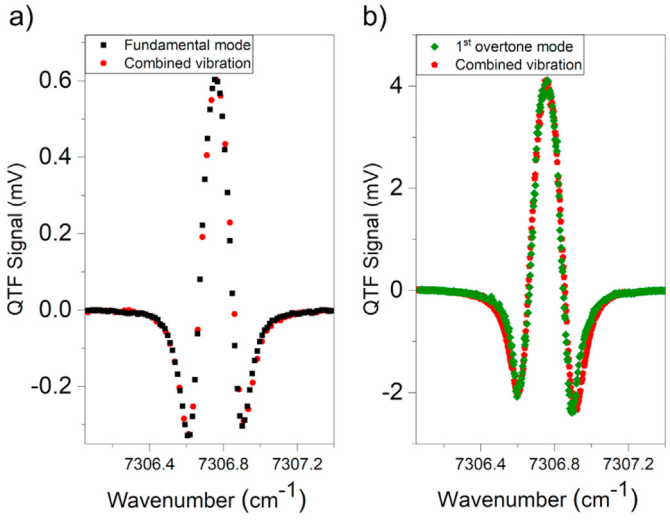

Fig. 4. QEPAS scans of a mixture composed of 1.6% H_2O in N_2. (a) QTF signals collected operating the resonator at the fundamental flexural mode (black squares) and combining both fundamental mode and 1st overtone mode (red dots). (b) QTF signals collected operating the resonator at the 1st overtone mode (green diamonds) and combining both vibrational modes (red dots). (For interpretation of the references to colour in this figure legend, the reader is referred to the Web version of this article.)

3.1. Sensors operating in the near-IR spectral region

The first multi-gas detection approach based on QEPAS technique was implemented by Frank Tittel's Laser Science Group, at Rice University. The first optical source used was a telecom laser diode. In 2006, a 2 μm thermoelectrically cooled DFB laser diode and a standard spectrophone were employed by Lewicki et al. in a benchtop QEPAS prototype to detect CO_2 and NH_3 [57]. The CO_2 target absorption lines were selected within R-branch of the $2\nu_1+\nu_3$ band and a bunch of NH_3 absorption features from the $\nu_3+\nu_4$ band were identified in the 4982 cm^{-1} to 4993 cm^{-1} range. At a pressure of 50 Torr, all the features belonging to both analytes were perfectly separated. The minimum detection limit for carbon dioxide was measured to be 18 ppm with a lock-in integration time $\tau = 1$ s, while for ammonia the MDL was measured as low as 3 ppm [57]. The influence of water vapor concentration on energy relaxation processes for both molecules was evaluated through the QEPAS signal amplitude and phase. A relaxation time constant k^{-1} of 3.53 μs atm was calculated for carbon dioxide in a CO_2:H_2O:N_2 mixture. In comparison to a previous investigation [31] in which a bare QTF was employed, the CO_2 relaxation rate related to dry gas was found > 3 times faster in the system employing the spectrophone with the ARs. The main reason behind this sensible reduction of the k^{-1} value was attributed to the energy relaxation of the CO_2 molecules via collisions with the resonator tube walls. In terms of humidity effect, for CO_2 detection a water vapor concentration increasing from 1.47% up to 3.1% leads to a 6.2% increase of the photoacoustic signal amplitude, representing a non negligible impact on the gas sensor prototype calibration. Whereas for ammonia no significant changes due to H_2O concentration were experimentally measured. Indeed, ammonia has been proved to rely on a fast V–T relaxation rate. Thus, the sound wave can be effectively generated also at modulation frequencies higher than 10 kHz and the photoacoustic signal are not affected by the water vapor concentration in the gas mixture.

Starting from the benchtop prototypes realized during the first decade of the new millennium, the Laser Science Group of Rice University has developed several compact units with integrated laser sources, electronics, and reference cells. Initially, the acoustic detection module was external to the unit and solid core fibers were connected to the system for delivering the laser beams at the ADMs (Fig. 5). The 1% of the laser radiation, obtained by a beam-splitter, was delivered to a reference cell filled with a gas target

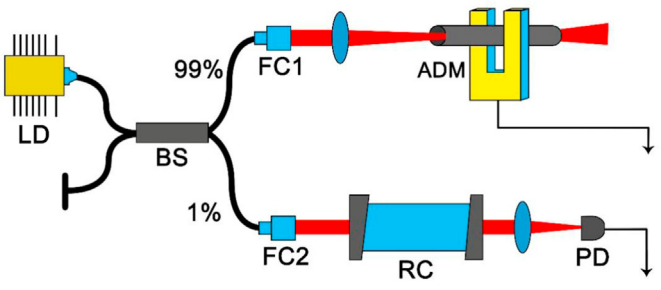

Fig. 5. Schematic of QEPAS sensing prototype employing a single diode laser. LD-laser diode; RC-reference cell; BS-beam splitter; ADM-acoustic detection module; FC1, FC2-fiber collimator; PD-photo detector.

concentration in the percent scale, with the specific goal of implementing absorption line-locking measurements. The locking loop was enabled through the 3*f*-detection of the absorption signal, monitored by means of a photodiode [58].

In 2008, a single distributed feedback diode laser (DFB-LD) operating at 1.53 μm and targeting NH_3, HCN and C_2H_2 within its dynamic range, was demonstrated by Kosterev et al. [59] to realize a trace gas sensor for early fire detection. In such a multi-gas sensor, the main criteria for implementing a simple scheme of independent detection require that the targeted absorption features should: i) lie within the tuning range of a DFB diode laser, which is in the order of ~15 cm^{-1} for operating temperature variations of 40 °C; ii) not exhibit a consistent overlap among them or with absorption spectral lines related to interfering species normally present in atmospheric air, like water vapor or carbon dioxide; iii) have the largest linestrength available for the molecule under investigation. These guidelines led to selection of the spectral lines falling at 6528.80 cm^{-1}, 6536.48 cm^{-1} and 6523.87 cm^{-1}, for NH_3, HCN and C_2H_2 detection, respectively. In this version of a QEPAS multi-gas sensor, a Control Electronics Unit (CEU) was used as commutator to drive the DFB-LD and to access the three target lines by means of a 3*f*-locking technique, in which the emission wavelength was sequentially fixed at the respective absorption peaks by monitoring the zero crossing 3*f* absorption signal through a reference cell. The laser working parameters and the signals from the photodiode, humidity, pressure, and temperature sensors were provided and stored by the CEU. The calibration of the sensor and performance assessment provided noise-equivalent concentrations of 100, 125 and 30 ppb for NH_3, HCN and C_2H_2, respectively, for 4 s data acquisition time at 450 Torr gas pressure. The interferences among the three analytes were evaluated by measuring the relative input from each of the three target molecules into each of the measurement channels. The cross-talk matrix, composed of the 1 ppm signal values for each molecule and the induced signal concentrations on the other detection channels, highlighted how the interference effect from each analyte on the others is at least 50 times weaker with respect to the 1 ppm signals [59].

A similar version of compact two-gas QEPAS sensor was developed by Dong et al. for trace methane and ammonia detection in impure hydrogen [60]. Two different laser diodes, targeting a CH_4 line located at 6057.1 cm^{-1} and a NH_3 line falling at 6528.7 cm^{-1} respectively, were employed. The single mode fibers connected with the two LDs were combined with a MEMS switch and delivered to an ADM, mounting a standard QTF spectrophone. With respect to previous investigations, in which methane or ammonia were detected with the same apparatus in a matrix of wet nitrogen [23], in a hydrogen-based matrix the QTF experienced a relatively high increase of the quality factor *Q* because of the lower molecular weight of the gas matrix. Indeed, the QTF quality factor ranges from 55,000 at 50 Torr down to 30,000 at atmospheric pressure in a hydrogen carrier gas environment, compared to values varying from 30,000 at 50 Torr down to 2000 at 1 atm in a N_2-based gas matrix. However, this effect was substantially compensated by the fact that the ARs mounted in the spectrophone were optimized for the sound wavelength in N_2 based mixtures, leading to a reduced enhancement of the QEPAS signal with respect to what achieved in N_2 matrix. It was also experimentally found that the addition of H_2O did not significantly promote vibrational relaxation of CH_4 in H_2, differently from the case of CH_4:N_2 mixture. Nevertheless, for H_2O concentrations >2000 ppm, a correction of the CH_4 measured concentration with respect to the H_2O content would have been necessary [60].

The most structured version of a portable near-IR QEPAS multigas sensor was conceived and realized by Dong et al. for the analysis of post-combustion products of materials for aerospace and space station environments [61], see Fig. 6. All the absorption features selected fall in the related overtone vibrational spectrum. For CO detection, the selected optimum target line falls at 4288.29 cm^{-1} (2.3 μm) with a linestrength of $3.47 \cdot 10^{-21}$ cm/mol. Due to the carbon dioxide background of ~370 ppm in ambient air, the CO_2 sensing channel did not need a high sensitivity, thus a line at 6361.25 cm^{-1} (1.57 μm) with a linestrength of $1.7 \cdot 10^{-23}$ cm/mol was used. For HCN, the absorption transition located at 6539.11 cm^{-1} (1.529 μm) having a linestrength of $6.8 \cdot 10^{-21}$ cm/mol was selected, while for HCl the absorption line falling at 5739.26 cm^{-1} (1.742 μm), characterized by a very intense linestrength of $1.25 \cdot 10^{-20}$ cm/mol with respect to the average linestrength in the overtone spectral region, was targeted [62]. Each analyte molecule had a dedicated diode laser and a standard spectrophone. All four sensing channels were mounted inside a compact CEU with dimensions of 10 × 25 × 25 cm. In this advanced version of the compact near-IR QEPAS sensor, the CEU was set to perform i) line-locked measurements, ii) QTF electrical characterization and iii) modulation of the LDs. The QTF electrical characterization consisted in providing a sinusoidal voltage signal to the resonator and, by varying the excitation frequency, retrieving the curve of the piezocurrent signal. This curve represents the resonance of the fundamental vibrational mode. The quality factor of the resonator was derived from the QTF ring-down time following a sudden interruption of the excitation voltage. Four sets of parameters were pre-programmed in the CEU, each set including a reference cell, the selected diode laser, its modulation depth, current and temperature, a spectrophone and control parameters. The system was also equipped with batteries so that the sensor could be able to independently operate for 8 h. All four ADMs had an open cell configuration to allow fast ambient air gas exchange with the internal sensor volume. The CEU was also equipped with a fan for heat dissipation.

All measurements were carried out at atmospheric pressure and the sensitivity achieved at 1 s integration time were 450 ppb for HCN, 7.7 ppm for CO, 100 ppm for CO_2 and 1.5 ppm for HCl, respectively. It was also verified that for all the four analytes, when the relative humidity is larger than 0.2%, the V-T relaxation rate is saturated and thus the humidity does not impact on the QEPAS signals [61].

3.2. Sensors operating in the mid-IR spectral region

With respect to the near-IR spectral region, where the overtone absorption bands of the molecules lie, in the mid-IR spectral region the fundamental absorption bands can be excited with linestrengths typically two orders of magnitude stronger than in the near-IR spectral region [63]. The demonstration of quantum cascade devices and the advances in quantum electronics at the turn of the millennium provided the spectroscopy research field with powerful laser sources, like QCLs and ICLs, for targeting the mid-IR spectral region [10].

The first multi-gas QEPAS sensor operating in the mid-IR was demonstrated in 2004 by Kosterev et al. [28], two years after the first demonstration of the QEPAS. The molecules targeted for this study were N_2O and CO. The interest in pursuing environmental trace gas detection of nitrous oxide consists in the fact that it represents one of the main contributors to the global greenhouse effect, with atmospheric concentrations ranging from 310 to 320 ppb and average growth rate of ~ 0.8 ppb/year [64]. Carbon oxide is the main pollutant found in industrial and urban atmospheres, with background levels of CO found in relatively unpolluted air range from 0.2 to 1.0 ppm, and represents also an essential biomedical marker in breath analysis for noninvasive diagnostics of diseases in medicine [2]. All these applications require better

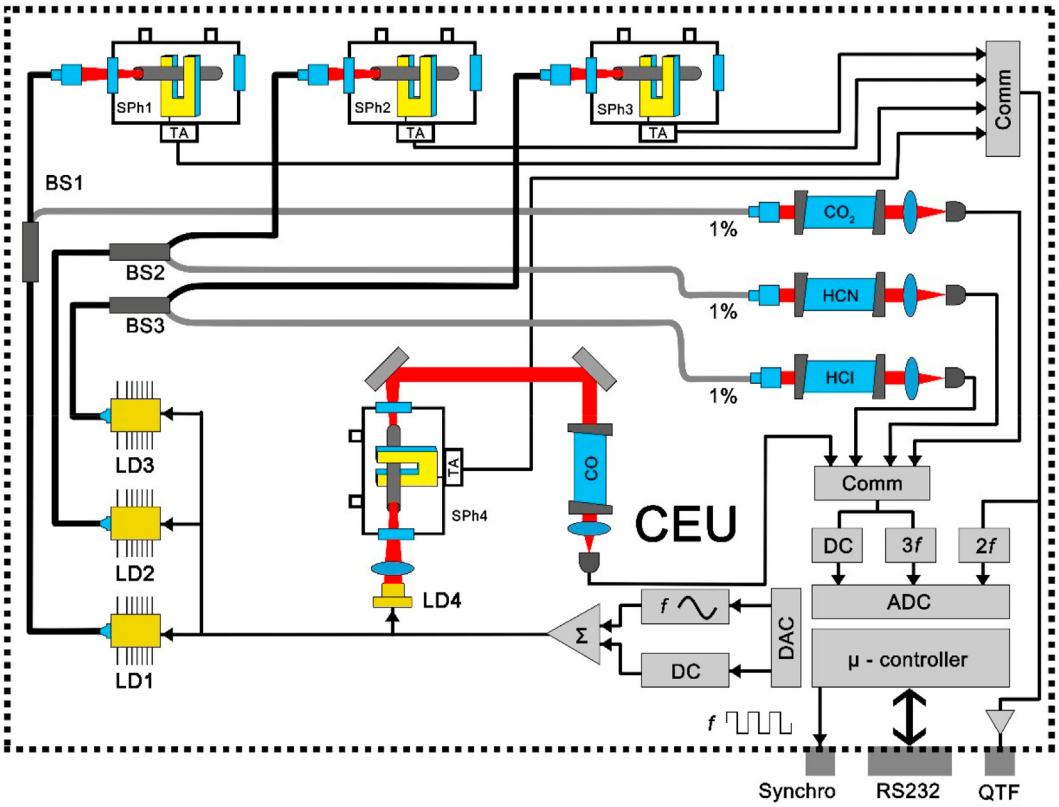

Fig. 6. Schematics of a multigas QEPAS sensor. With respect to Fig. 5, CEU is the control electronics unit, while SPh1, SPh2, SPh3, SPh4 are the spectrophones employed; TA stands for transimpedance amplifier.

sensing capabilities with respect to those reached by QEPAS sensors operating in the near-IR spectral region. For this first mid-IR multigas QEPAS sensor targeting N_2O/CO, Kosterev et al. employed a continuous wave, distributed feedback QCL (CW DFB-QCL) as a photoacoustic excitation source. This laser was liquid-N_2 cooled and was able to cover the spectral range 2198.3–2195.5 cm^{-1} (4.55 μm). A standard QTF spectrophone was used in this experiment. The QEPAS measurements were performed in two modalities: i) scan mode, in which the laser injected current is slowly varied to obtain a wavelength emission scan across the spectral window under investigation, and ii) line-locking mode, where the amplitude of the 3*f* component of a direct absorption signal from the reference cell was measured via a IR detector, in order to maintain its value set to zero and provide a proportional correction to the dc component of the laser current. Therefore, the laser emission wavelength was locked to the peak of the selected absorption feature. In order to detect nitrous oxide, the P(30) transition of the ν_3 mode at 2195.633 cm^{-1} was targeted. Carbon monoxide detection was carried out exciting the R(14) line located at 2196.664 cm^{-1} [62]. The linestrength of the accessible CO absorption feature was almost two times less intense than the one used for N_2O. Concentrations ranging from 0 up to 8% of sulfur hexafluoride were added to air with the aim of promoting the V-T energy relaxation of the N_2O vibrational state excited. SF_6 exhibits a high density of vibrational levels, opening many different pathways to relax energy through collisions and creating a ladder for an efficient multistep relaxation [41]. Indeed, the presence of SF_6 in the matrix determined significantly higher QEPAS signals recorded for N_2O: a 0.5% addition of SF_6 provided a 5.7 times signal amplification. A SF_6 concentration > 30% determined on the other hand a decrease in the QEPAS signal because of: i) the dilution of the gas sample; ii) the ARs' resonance detuning from the demodulation frequency f_0 caused by the variation of the sound speed in the mixture; iii) the increased thermal capacity of the carrier gas; iv) the decrease of the QTF's quality factor, dropping from 26,600 in pure N_2 down to 10,800 in pure SF_6 at 50 Torr. The optimum SF_6 concentration for the N_2O photoacoustic detection was found to be 5%. Such a SF_6 addition provided an order of magnitude signal enhancement compared to a N_2O signal in N_2. At an operating pressure of 50 Torr and a lock-in time constant of $\tau = 3$ s, the N_2O QEPAS signal linearity was demonstrated and a MDL of 4 ppb was achieved. The QEPAS signal acquired by exciting the R(14) transition of carbon monoxide, in a matrix of pure nitrogen at a pressure of 50 Torr, was measured as low as 35 times weaker with respect to the signal obtained by an equivalent absorbing concentration of N_2O in N_2:5%SF_6. As a consequence, the sensitivity of the QEPAS sensor in detecting CO was estimated as 70 times worse with respect to its capability of detecting N_2O. Differently from N_2O photoacoustic response, the addition of sulfur hexafluoride up to 10% of the volume did not give rise to an improvement in sensitivity. The response of the sensor to CO followed the decrease of the QTF quality factor, for a total pressure increasing up to 1 atm. Thus, the MDL for CO detection at $\tau = 3$ s was 280 ppb, not sufficient enough to monitor atmospheric CO, also because of the relatively low optical power (< 20 mW) provided by the QCLs available at that early stage of development.

As a further evolution of the N_2O/CO sensor, Y. Ma et al. demonstrated a more compact QEPAS prototype using a high power CW DFB-QCL (~1 W) emitting at 4.61 μm and operating at 10 °C [65]. The WM and a *2f* demodulation allowed a reduction of the sensor background noise and, combined with the high optical power employed, MDL values suitable for environmental detection

of CO and N_2O were reached. The detection system was operated in continuous scan mode as well as in line-locking mode with 1 s of acquisition time. A minimum detection limit of 1.5 ppb at the atmospheric pressure was demonstrated for the CO line located at 2169.2 cm^{-1}, running the sensor in scan mode. An MDL of 23 ppb at 100 Torr was calculated for the N_2O line falling at 2169.6 cm^{-1}. Moreover, the Allan-Werle deviation analysis for environmental data provided a MDLs for N_2O and CO of 4 ppb and 340 ppt, respectively, at 500 s integration time [66]. With the aim of performing out-of-lab environmental measurements, the sensor platform was enclosed in a box measuring 12 × 5 × 5 inches, with a weight of ~4 kg and powered by a CEU requiring ~50 W of electrical power. The response time was kept low enough (<5 s) thanks to an ultra-compact ADM with the related low detection volume. The continuous monitoring of atmospheric CO and N_2O concentration levels for >5 h demonstrated the stability and reliability of the QEPAS sensor system, as well as its suitability for real time and in-situ trace gas detection [65].

This goal was finally achieved by Jahjah et al. who realized a portable mid-IR QEPAS sensor for N_2O/CH_4 detection in 2013. The developed QEPAS sensor was tested in a mobile laboratory (AML) provided by Aerodyne Research, Inc. to perform continuous, atmospheric CH_4 and N_2O measurements nearby two landfills, Atascocita and BFI McCarty, in the northeastern area of Greater Houston [67]. The employed laser source was a CW DFB-QCL emitting at 7.83 μm, while a standard spectrophone was employed. The targeted CH_4 and N_2O absorption lines were located at 1275.04 cm^{-1} and 1275.49 cm^{-1}, respectively. In this wavenumber range, the N_2O and CH_4 absorption linestrengths are $1.407 \cdot 10^{-19}$ cm/mol and 3.729n10^{-20} cm/mol, respectively [62]. These linestrengths combined with a powerful (>120 mW) laser source employed in the QEPAS sensor system provided an excellent MDL of 13 ppb for CH_4 and 6 ppb for N_2O, at 1 s integration time. In order to avoid the CH_4 signal dependence on atmospheric water vapor fluctuations, a Nafion tube was used to humidify the sample air and saturate the relaxation rate of methane. The QEPAS sensor measurements were validated by comparing them with data simultaneously recorded by an Aerodyne Research, Inc. ultrasensitive sensor system based on a QCL and a multi-pass cell [68]. Enhancements of ~30 ppb of N_2O and ~8 ppm of CH_4 with respect to their natural concentrations were detected when the AML was stationing nearby the landfills or driving around them at a distance of ~200 m. The CH_4 and N_2O atmospheric concentrations returned to background levels when the circling distance exceeded ~400 m because of dilution. Furthermore, the sensor clearly detected peaks of CH_4 and N_2O concentration as a result of waste trucks driving close to the AML [67].

3.3. Sensors devoted to isotopic ratio measurements

The detection of isotopologues is a very delicate application, especially if the designated detection technique is based on the photoacoustic effect. It is extremely advisable for any optical technique that the energy difference between the two excited transitions is sufficiently large in relation to the their own linewidth to ensure a good separability of the two features [69,70]. In particular, when the determination of isotope ratios is pursued through the photoacoustic approach, in addition to a highly selective detection, it is essential that the gaseous matrix does not experience significant variations. For this reason, until now, the only evidences of isotope ratio measurements via QEPAS were demonstrated for gas traces in a fixed matrix [69–71]. High precision isotope ratio measurements require a spectral separation of the absorption lines large enough to avoid that, at a given operating pressure, absorption interference occurs. The abundance ratio for a pair of isotopes in a sample gas is usually expressed in relation to a reference mixture gas as a δ-value, which is defined as

$$\delta = \left[R_{sample} \Big/ R_{reference} - 1 \right] \times 1000‰ \quad (9)$$

where R_{sample} and $R_{reference}$ are the concentration ratio between the two isotopes in the sample and in the reference gas, respectively and δ is expressed in parts per thousand.

In the case of methane isotopes, both $^{12}CH_4$ and $^{13}CH_4$ are spherical rotors exhibiting similar schemes of ro-vibrational lines, just separated by ~10 cm^{-1} because of the C mass difference [72]. For $^{13}CH_4/^{12}CH_4$ features having comparable linestrengths, the main difficulty in evaluating the isotopic ratio comes from the large difference in isotopic abundances, which is ~1/100. As a consequence, the most desirable pair of target lines should have a $^{13}CH_4$ line-strength ∼ two orders of magnitude higher with respect to $^{12}CH_4$ transition linestrength to balance out the disparity in abundance. The cross-section ratio dependence on the temperature is another fundamental aspect to be carefully assessed by evaluating the broadening coefficients and the ground-state energies. In fact, the lower energy levels should be close with the same quantum numbers. With the aim of fulfilling these requirements, Sampaolo et al. identified the lines located at 1296.12 cm^{-1} for $^{12}CH_4$ and 1296.03 cm^{-1} for $^{13}CH_4$ [69]. For this experiment a CW DFB-QCL emitting at 7.73 μm was employed, targeting the core of the C—H bond bending bands [62]. The resonator selected was a T-shaped custom tuning fork having a 0.8 mm prong spacing to accommodate a ~300 μm QCL beam waist [24]. The resonance frequency was measured to be 12461.22 kHz while the quality factor was >40,000 at an operating pressure of 50 Torr. A pair of AR tubes, with an internal diameter of 1.52 mm and a length of 9.5 mm, were also coupled to the QTF in on-beam configuration. The absorption cross-sections for $^{13}CH_4$ and $^{12}CH_4$ at 50 Torr, simulated from the HITRAN database [62], are plotted in the lower graph of Fig. 7.

The absorption cross-section reflects also the natural abundance of $^{12}CH_4$ and $^{13}CH_4$, which are approximately 98.82% and 1.11%, respectively. The temperature changes were estimated to affect the cross-section ratio at 20 °C, which was calculated to be σ_{13}/σ_{12} ~ 0.06, with a coefficient of −6.7‰/°C. This correction was assumed to be not impacting on the experiment because of the thermal stability of the overall apparatus. In the upper panel of Fig. 7, the *2f*-QEPAS scan acquired at 50 Torr for a mixture of 500 ppm CH_4:N_2 is shown. It can be noticed that the two features related to the isotopes $^{13}CH_4$ and $^{12}CH_4$ are easily recognizable. Different mixtures of methane, with unknown concentrations of $^{13}CH_4$ and $^{12}CH_4$, diluted in pure N_2 from 1000 ppm down to 50 ppm were analyzed. A perfect linearity of the *2f*-QEPAS signal peaks for both $^{12}CH_4$ and $^{13}CH_4$ was demonstrated. The σ_{13}/σ_{12} ~ 0.06 calculated from the HITRAN database found a perfect match with the *2f*-peak signals ratio S^{13}/S^{12} for each methane dilution, demonstrating that the actual concentrations of $^{13}CH_4$ and $^{12}CH_4$ in the gas sample are consistent with the natural abundances reported in the Hitran database [62]. In order to estimate the sensor capability of detecting $\delta^{13}C$ variation at a given integration time, the uncertainty $\Delta\,\delta^{13}C$ on $\delta^{13}C$ was calculated through the propagation of error applied at Eq. (9). For a mixture of 1000 ppm CH_4:N_2, $\Delta\delta^{13}C$ resulted in the order of 10‰ at an integration time constant of 0.1 s. For a methane gas mixture in the percent concentration scale, typical of natural gas samples, and at an integration time of 1 s, the $\Delta\delta^{13}C$ is expected to reach a value well below the 1‰ usually required for this kind of isotope analysis [69].

With the same criteria Z. Wang et al. identified spectral features for CO_2 isotopes detection for medical applications, realizing a sensor with a CW DFB interband cascade laser (CW DFB-ICL) [71].

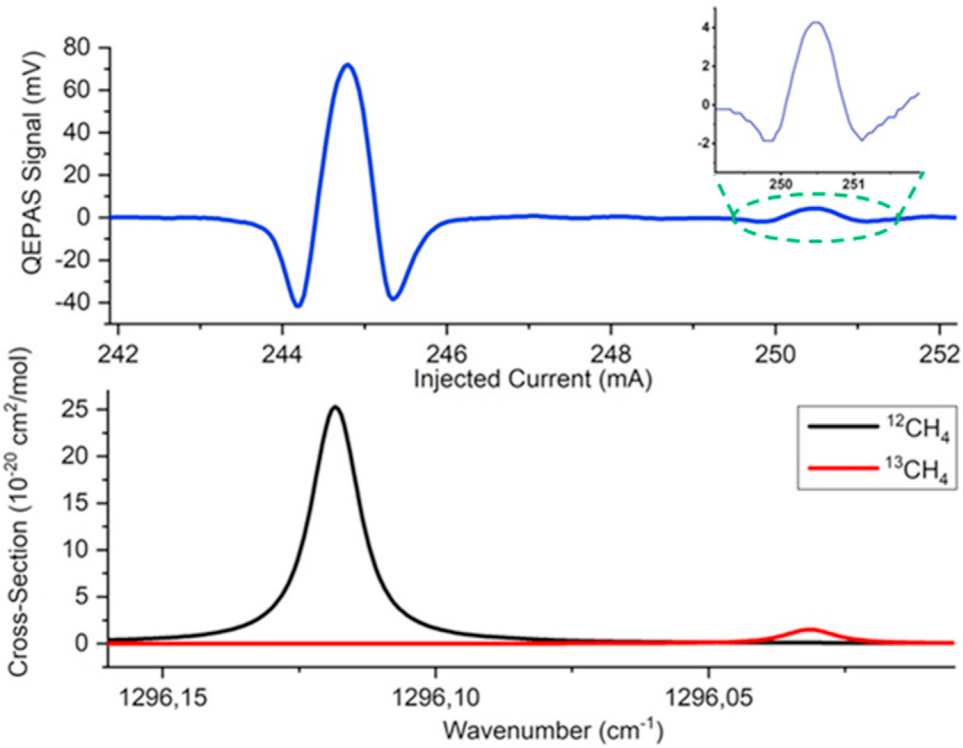

Fig. 7. Lower panel: cross-section at 50 Torr for $^{13}CH_4$ (red line) and $^{12}CH_4$ (black line) absorption lines. Upper panel: 2f-QEPAS signal recorded for standard methane at a concentration of 500 ppm:N_2 at 50 Torr. The QCL injected current scan in the upper x axis matches the wavelength range shown in the lower x-axis (1296–1296.15 cm^{-1}). A zoom on the ^{13}C peak is shown in the inset. (For interpretation of the references to colour in this figure legend, the reader is referred to the Web version of this article.)

They employed an ICL emitting an optical power <2.6 mW at 4.35 μm and targeting the R(18) line of $^{13}CO_2$ and the P(43) and P(44) lines of $^{12}CO_2$, within a single current scan. The laser beam was coupled into a 100 μm solid-core indium fluoride optical fiber reaching an 88% optical coupling efficiency. The single-mode fiber output was then coupled into a standard QTF-based spectrophone in off-beam configuration. The measurements were carried out implementing WM with 2*f* demodulation. The sensor was able to analyze the CO_2 isotope ratio with an average precision <1‰ at a 700 s lock-in integration time, which represents a suitable result for targeting most of the medical and biomarker-based applications [71].

The most precise approach to assess isotope ratio analysis was proposed by Spagnolo et al. for $^{18}O/^{16}O$ ratio measurements in water vapor, implementing a modulation cancellation method to reduce the background noise [70]. The modulation cancellation method (MOCAM) was introduced as a further development of the modulation spectroscopy approach based on two laser sources. The principle of operation for MOCAM exploits the fact that the modulation phases and the powers of two laser sources can be adjusted to level off the background signal affecting the measurement accuracy [73]. MOCAM can be implemented in different configurations including wavelength modulation combined with *1f* or *2f* demodulation. This technique applied to QEPAS was proven to efficiently i) sense temperature differences in a gas samples [74], ii) monitor isotope ratios [70] and iii) perform broadband detection at atmospheric pressure [13]. The scheme of the MOCAM-QEPAS architecture implemented by Spagnolo et al. for monitoring the isotope $^{18}O/^{16}O$ ratio in water vapor is depicted in Fig. 8.

Two diode lasers were wavelength modulated at the same frequency and the combined beam was split in two and then delivered to two ADMs, one containing the reference sample (RGS) and the other with the gas to be analyzed (AGS). The wavelength of both lasers was locked to the absorption lines related to the isotopologues $H_2^{16}O$ and $H_2^{18}O$. The optical power and modulation phase were manually adjusted in such a way that the *2f*-QEPAS signals generated by the two LDs were identical and opposite in phase. The phase relations were kept constant by a phase-locked loop. In this way, the two photoacoustically generated signals in the RGS could be balanced out and the QTF detected no signal with an uncertainty equal to the thermal noise of the resonator. For this condition, the analyzed sample signal resulted to be directly proportional to the deviation of the linestrength ratio from the reference ratio in the designated optical configuration. The sensitivity achieved in determining the deviation from a standard sample $\delta^{18}O$ was 1.4‰, at 200 s of lock-in integration time [70].

4. Trace gas detection of broadband absorbers

Spectroscopic techniques based on light absorption require the selection of absorption lines isolated from other spectroscopic features and with a negligible background, to guarantee high selectivity and sensitivity. Such a condition can be usually fulfilled for molecules composed of less than five atoms while the high density of vibrational states, combined with the broadening of absorption lines, leads to structured absorption features spreading over a wide spectral range. This is the case of complex molecules, such as volatile organic compounds (VOCs) [63]. When the absorption bands of the major constituents of the gas matrix give rise to a continuum-background, impurities or trace gases can be hardly detected. Therefore, additional parameters and tools are needed to correctly identify absorption features and measure the concentrations of the gas components.

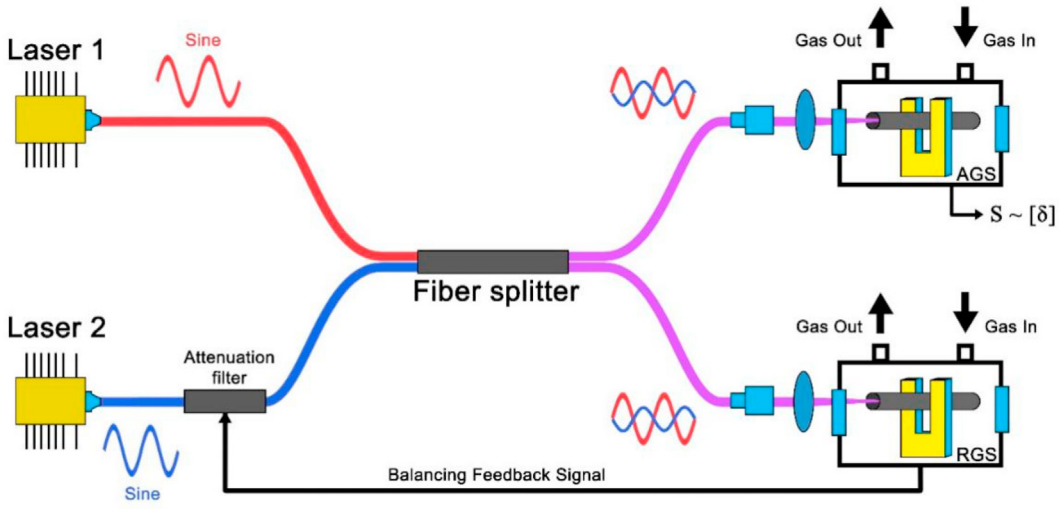

Fig. 8. Schematic of the MOCAM-QEPAS apparatus setup for monitoring isotope ratios. RGS is the reference gas sample, while AGS is the analyzed gas sample.

4.1. Role of detection phase in multi-component gas analysis

In paragraph 2.3, the significant differences in photoacoustic response due to the relaxation rates of different target molecules in a given mixture were described. This condition, that typically complicates the QEPAS signal interpretation when gas matrix variations occur, can be used on the other hand to enhance the chemical selectivity of measurements. In fact, the shift in phase of the photoacoustic response to the modulated excitation can be exploited to determine the V–T relaxation rate. For a two-level molecular system, the photoacoustic phase lag θ is determined by Ref. [75]:

$$\tan(\theta) = \omega\tau(C_{T-R} / C_0) \quad (10)$$

where τ represents the V–T relaxation time, ω is the modulated excitation frequency, $C_{T\text{-}R}$ is the translational-rotational heat capacity, and C_0 is the total heat capacity, both at constant volume. Equation (10) was first verified experimentally for a two-level system and then generalized for multilevel and multispecies systems [76,77].

The photoacoustic phase selective detection (PPSD) was employed for the first time to identify the absorption features of the components in a multi-gas mixture by Kosterev et al. [75]. In this study, each n-th gas species photoacoustic signal is represented by a rotating vector $\boldsymbol{A}$ in a phasor diagram, having a complex amplitude $A_n \exp(i\alpha_n)$, with $n = 1, 2$. Experimentally, the projections of the sum of these rotating vectors on the x-axis and on the y-axis correspond to the lock-in amplifier quadrature components (X and Y) when the phase is referenced to the laser driver modulation input. The phase angle α_n depends on the photoacoustic phase lag θ_n defined in Eq. (10) and on the phase shifts contribution introduced by electronics, laser and quartz tuning fork. If the frame of reference is rotated till the y'-axis is parallel to the vector $\boldsymbol{A}_1$, the quadrature component X will correspond to the projection on the x′-axis of the vector $\boldsymbol{A}_2$. In this way the signal of the gas species 2 can be detected without any interference due to the signal of the gas species 1.

Kosterev et al. applied the PPSD to detect impurities of carbon monoxide (CO) in propylene (C_3H_6) [75]. The C_3H_6 molecule exhibits a broad absorption band spreading in the whole mid-infrared spectral range. When mixed with propylene, CO is hardly detectable by using a laser absorption-based technique, since its absorption features are embedded into the C_3H_6 absorption continuum-background [62]. In Ref. [75] a liquid N_2-cooled continuous wave DFB-QCL was employed as the light source, whose wavenumber was tunable in the 2195.5–2198.2 cm^{-1} range, with an emission power of about 10 mW at 2196.664 cm^{-1}, corresponding to the carbon monoxide R(14) transition [62]. The resonator employed was a standard QTF spectrophone and a WM approach combined with *2f* demodulation was adopted for measurements. A sample of propylene with 4.99 ppm of CO was tested in this experiment. The QEPAS spectral scan acquired at a pressure of 50 Torr, with an integration time of 1 s, is shown in Fig. 9a.

When the lock-in phase is fixed to 0°, the signal corresponding to the carbon monoxide absorption line cannot be distinguished over the C_3H_6 background (Fig. 9a). If the frame of reference is rotated with an angle of 22°, the X component contains only the signal arising from the CO excitation (Fig. 9b), which can be detected with an SNR = 50. The propylene phase α_1 can be calculated as $\alpha_1 = 22° + 90° = 112.3°$. The same measurements were repeated for different gas mixture pressures, between 30 Torr and 150 Torr. A working pressure of 50 Torr was found to maximize the carbon monoxide signal component orthogonal to the propylene signal.

Similar investigations were carried out by Wang et al. for C_2H_4 detection by using a CW DFB-QCL with central wavelength emission at 10.5 μm and a standard spectrophone [78]. In this case, a detailed study of pressure and phase was carried out to detect ethylene (C_2H_4) in a matrix of interfering carbon dioxide (CO_2). Sensor calibration showed a good linearity of the responsivity against the ethylene concentration, with a MDL of 8 ppb, for 90 s of lock-in integration time [78].

4.2. Analysis of overlapping absorption spectra exploiting a single DFB laser source

Several approaches have been discussed so far to detect the components in a multi-gas mixture. In the simple case of isolated absorbing features, spectrally separated of few cm^{-1}, the full dynamic spectral range of a single light source can be exploited. In the case of isolated absorbing features, spectrally far from each other, several light sources can be employed, each one to detect a single gaseous component [61]. In this approach, the lasers can be operated in sequence or, for a two-component mixture, simultaneously,

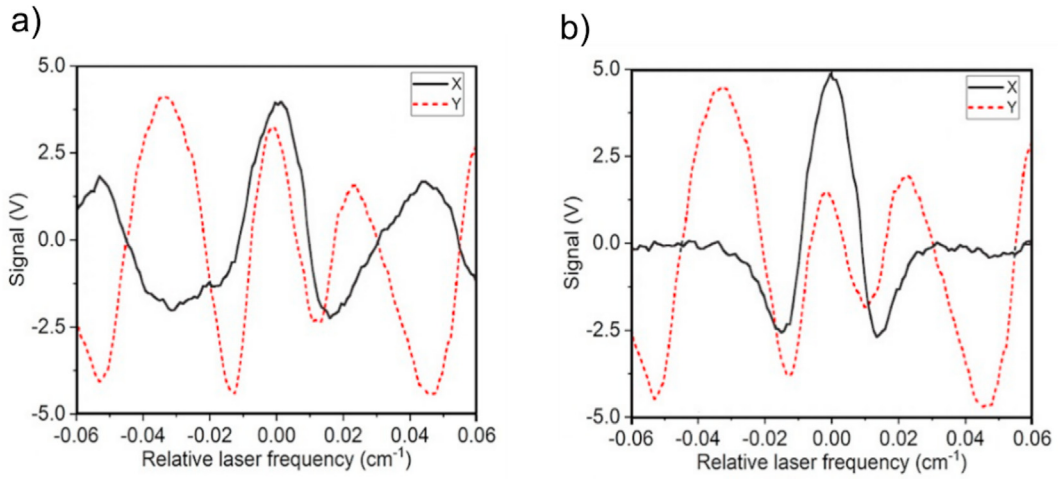

Fig. 9. a) X and Y component of the QEPAS spectral scan for a sample of propylene with an impurity of 4.99 ppm of CO, acquired with 0° phase on the lock-in; b) X and Y component of the QEPAS spectral scan for the same sample, with a lock-in phase of 22°.

each one exciting a quartz tuning fork in-plane resonance mode [38]. However, in all the examples provided until now, each gas component does not spectrally interfere with the others or, alternatively, it was possible to achieve non-interfering independent detection by selecting a suitable operating pressure and/or by properly tuning the detection phase. A different approach must be used in the case of absorption spectra resulting from different gases overlapping features. Here, the contribution from different components can be identified only by using multivariate analysis (MVA) [79]. Usually, among the MVA approaches, the multilinear regression (MLR), i.e., the extension of the linear regression to multiple variables, is employed. In MLR, ordinary least squares method is used to predict a dependent variable, i.e., the target molecule concentration, from a set of independent variables, i.e., the acquired spectroscopic signals. Such an approach is reliable in the case of uncorrelated low-noise data, while correlated variables would increase the uncertainties of the predicted results. Therefore, in the case of complex systems whose spectral features overlap, these requirements cannot be guaranteed, thus leading to a lack of precision and accuracy of the MLR model. Moreover, if some interaction among the target analytes occurs, this can lead to matrix effects influencing the spectroscopic signals. In such a case, the relationship among the dependent and the independent variables is no longer linear, and cannot be modeled using MLR [80]. Furthermore, overfitting issues can arise because of the numerous variables involved [81]. In Refs. [82,83], QEPAS sensors are employed to detect analytes having overlapping absorption features, whose concentrations are retrieved by MLR. Both in Refs. [80,81], MLR results in a significant prediction error. Therefore, spectroscopic techniques based on laser absorption should exploit more advanced analysis tools to retrieve the contribution from a single component in a multi-gas mixture. With this aim, partial least squares regression (PLSR) has been introduced.

4.2.1. Hydrocarbon trace gas detection through MLR

The monitoring of hydrocarbons such as methane (CH_4), ethane (C_2H_6) and propane (C_3H_8) represents one of the most relevant application in gas sensing. For the petrochemical industry, hydrocarbon detection is an important tool to identify the gas origin and predict the presence of petroleum reserves [69]. Moreover, additional information can be retrieved by analyzing the hydrocarbons isotopic ratio. In particular, the origin of natural gases (biogenic or thermogenic) can be identified by measuring the isotopic ratio of carbon and hydrogen in methane [72]. Natural gas components analysis is one of the most challenging fields for gas spectroscopy, because of the huge absorption backgrounds from high concentrations of hydrocarbon molecules. This issue requires the smartest use of all the analysis tools and approaches introduced in the previous paragraph. In some cases, it could be convenient to dilute natural gas samples so that the principal components of the mixture such as CH_4, C_2H_6 and C_3H_8, usually measured at the percent scale, can be more easily detected in traces within a simpler and non-fluctuating gas matrix of inert gas such as N_2. However, the problem of spectral interference among alkane molecules, all characterized by the stretching of the C—H bond and having the fundamental bands in the 3—4 μm spectral window, still stands. In the overtone range (1—3 μm) also, the absorption features of a structured molecule like ethane display a broadband characteristic. Menduni et al. reported recently on a QEPAS sensor for sequential detection of environmental CH_4 and C_2H_6 to be employed in mobile or UAV-assisted monitoring systems [84]. The sensor is based on a fiber-coupled acoustic detection module and two laser diodes (LDs) with a center emission wavelength of 1653.7 nm (LD1) and 1684 nm (LD2) and an emission optical power of 12 mW and 8.5 mW, respectively. LD1 was employed to target a merged triplet of CH_4 (P1) around 6046.94 cm^{-1} having an overall cross-section of ~ $1 \cdot 10^{-20}$ cm^2/mol at 760 Torr [62]. LD2 was employed to target i) a merged sextet of CH_4 (P2) around 5938.12 cm^{-1} having an overall cross-section of $7 \cdot 10^{-21}$ cm^2/mol at 760 Torr [62] and ii) several C_2H_6 absorption features [85], showing the highest intensity peak (P3) at 5937.3 cm^{-1} [86—88]. Fig. 10 shows a sequential acquisition of the QEPAS signal at 760 Torr recorded with LD1 and LD2 (black and red solid line, respectively) for a gas mixture composed of 1% of C_2H_6 and 99% of N_2.

The background signal due to QTF thermal noise, sensor electronics and possible photothermal signal caused by the laser beam on the spectrophone, can be measured in the 0—140 s time window of the first wavelength scan and results to be lower than 0.15 mV. The rest of the signal is related to broadband structures, including the strongest P3 peak used for calibration. By selecting the proper detection phase, the authors were able to reach a condition of non-interference between the ethane absorption backgrounds and the near methane peak P2 as shown in Fig. 11.

Absorption features P2 and P3 can be clearly recognized in the QEPAS spectral scan in Fig. 11a. Moreover, by comparing the methane spectral scans in Fig. 11b, it can be noticed that the C_2H_6

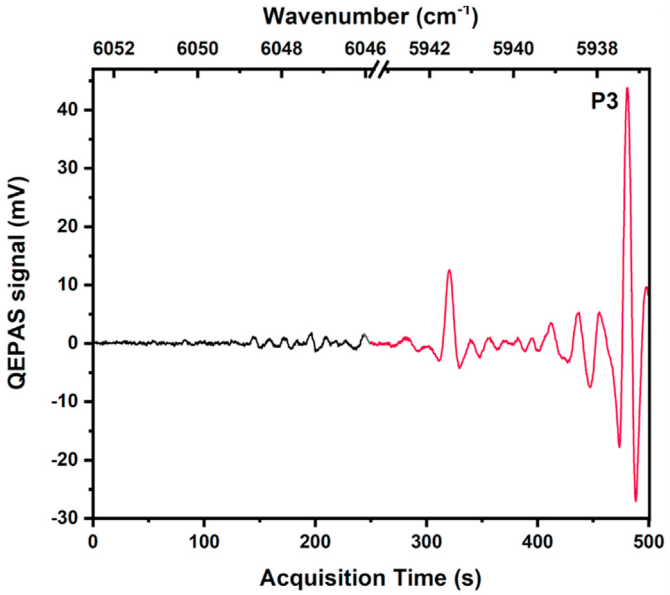

Fig. 10. QEPAS spectral scan of a mixture composed of 1% C2H6 and 99% N2, measured by sequentially scanning the LD1(black line) and the LD2 (red line) dynamic range. (For interpretation of the references to colour in this figure legend, the reader is referred to the Web version of this article.)

broadband absorption feature P3 influences the P2 profile only far from the peak. Therefore, it can be concluded that a measurement of methane concentration based on the QEPAS signal peak values is not influenced by the presence of C_2H_6, even for ethane concentrations almost ten times larger than the methane concentration to be retrieved, which is an improbable situation for natural gas leaks dispersed into the air.

In order to target the fundamental bands of the alkanes in the spectral range between 3 μm and 4 μm, ICLs are the most suitable laser light sources. Sampaolo et al. developed in 2019 a trace gas QEPAS spectrometer for methane, ethane and propane detection [82]. The selected ICL had a center emission wavelength at 3.345 μm and allowed the 2986.25 cm^{-1} absorption line of C_2H_6 and the three partially overlapped lines of CH_4 around 2988.8 cm^{-1} to be targeted [62]. Thanks to a spectral distance greater than 2 cm^{-1}, any overlap of the absorption features related to the two gases is avoided and a selective detection can be guaranteed for both analytes. The resonator employed in this spectrometer was a standard QTF spectrophone and a WM-*2f* demodulation was implemented. A good linearity was demonstrated for both molecules and a MDL of 90 ppb and 7 ppb were calculated via Allan deviation analysis for CH_4 and C_2H_6, respectively, at a lock-in integration time of 1 s [82]. The spectrometer was set to work with a simple and effective two-window CH_4/C_2H_6 detection scheme, by performing two fast and narrow scans around the selected features. Independent detection was demonstrated for both analytes, with a sensitivity lower than the part-per-million in concentration. The analytes concentration was demonstrated to be correctly retrieved in unbalanced mixtures, with a methane concentration ten times higher or even more than the ethane one. In this context, the non-zero C_2H_6 absorption background is not an issue for CH_4 detection also thanks to a proper detection phase selection.

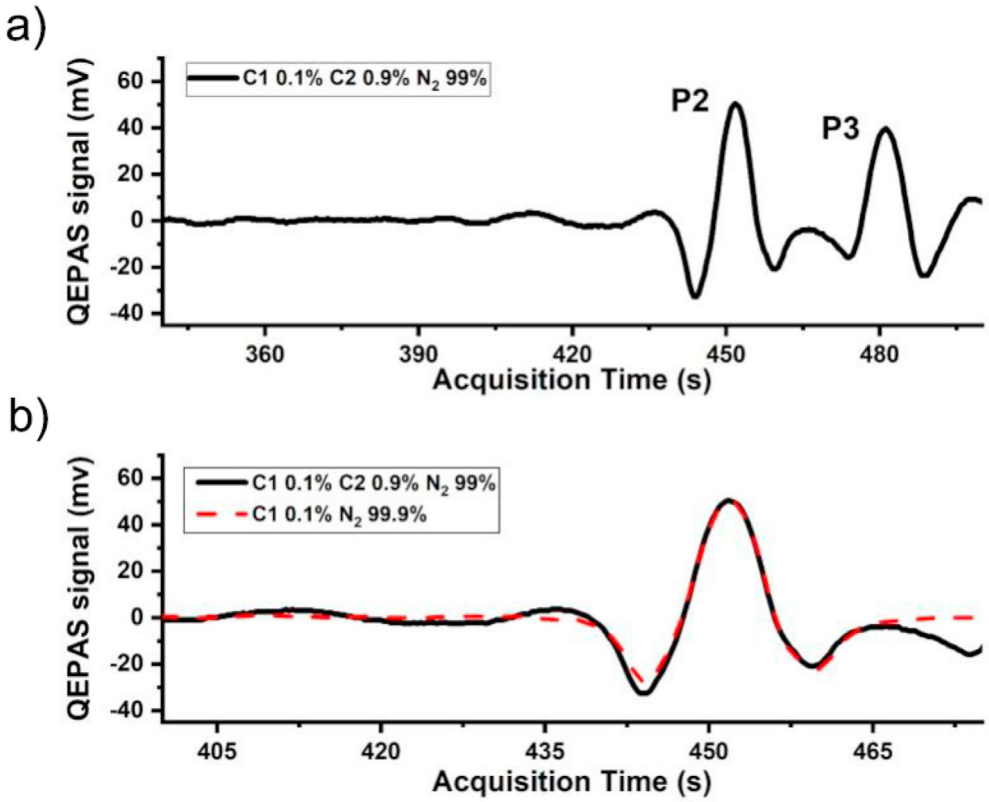

Fig. 11. (a) QEPAS spectral scan measured for a mixture of 0.1% CH_4 (C1 in figure), 0.9% C_2H_6 (C2 in figure) and the remaining 99% of N_2, by shining LD2. (b) P2 QEPAS spectral scan measured for a mixture of 0.1% and 99.9% N_2 (red dashed line), and 99% N_2 and 0.9% of C_2H_6 (black continuous line). (For interpretation of the references to colour in this figure legend, the reader is referred to the Web version of this article.)

In natural gas samples, starting from the ethane itself, the presence of more structured alkanes (like propane, butane etc.) introduces a higher overlap among the absorption features and leads to more broadened absorption spectra. For example, propane shows a structured absorption band in the spectral range from 3 μm to 4 μm, resulting from two transitions related to the stretch of the CH_3 groups and one transition related to the stretch of the CH_2 group. In Ref. [89] widely tunable OPO light sources were used to reconstruct the described C_3H_8 absorption band exhibiting a sharp peak at 3369.76 nm. In Refs. [67,80] an ICL was employed in a QEPAS system aiming at propane detection in the 3 μm−4 μm spectral range. Ethane absorption features within the typical ICL spectral emission range have cross sections at least five times stronger than propane ones [62,69,82]. However, at pressures comparable to the atmospheric one, absorption lines broaden and, due to their small spectral distance, give rise to the merging of multi-structured features. In Refs. [67,80] QEPAS spectra of propane, diluted in nitrogen to achieve concentrations in the range 100 ppm−1000 ppm, were acquired. The spectrum corresponding to 1000 ppm of propane was assumed as reference ($R_{1‰}^{C3H8}$) and all the other spectra were fitted with a function $S = c\,R_{1‰}^{C3H8}$, where the fitting parameter c represents the amount of propane in the mixture, divided by 1000 ppm. A linear sensor responsivity was proved, and the MDL estimated for an integration time of 100 ms was 3 ppm. Then, the MLR analysis tool was implemented to discriminate signals from C_2H_6 and C_3H_8, having overlapped features within the investigated spectral range. Different mixtures containing the two analytes (in concentration between 100 ppm and 1000 ppm) and nitrogen were obtained by using a gas mixer. The QEPAS spectral scans were analyzed by using a linear combination of the reference spectra, $R_{1‰}^{C3H8}$ and $R_{1‰}^{C2H6}$, respectively:

$$S = c\,R_{1‰}^{C3H8} + c'\,R_{1‰}^{C2H6} \tag{11}$$

The C_2H_6 and C_3H_8 concentrations calculated from the parameters c' and c in Eq. (11) differed from the nominal concentrations by less than 5%, for all the mixtures. The obtained results represented the basis for a more complex study of natural gas-like samples with concentrations in the percent scale for each component. A detailed discussion will be given in Section 5, where the gas matrix effect will be also addressed.

4.2.2. Multi-component mixtures analysis through MLR and PLSR: a comparison

Partial least squares regression (PLSR) is a widely used method for multivariate regression analysis and its application spans from spectroscopy and chemometrics to economic science [90]. Compared to MLR, PLSR is able to analyze experimental data having a large number of variables which are noisy and highly correlated [80]. A proper modeling of the interaction among the target analytes can be carried out, leading to an accurate retrieval of the single gaseous components' concentration. PLSR projects the system under investigation on a set of latent variables (LVs) truly independent [91]. In PLSR, predictors-matrix **P** and dependent variables-matrix **D** are defined as the matrix of the experimental data (i.e., the QEPAS spectra) and the matrix of the variables to be retrieved (i.e., the gaseous components and their concentration), respectively. The covariance matrix between **P** and **D** must be maximized for producing more stable results with respect to other regression tools [92]. In PLSR predictive analysis applications, data are split in training/test sets, as in the machine learning approaches. For multi-gas detection applications, the training set calibrating the model is based on the spectra acquired for a single target molecule, as a reference. A regression matrix is then calculated, to estimate gaseous components concentration.

A. Zifarelli et al. published a study in which for the first time PLSR was applied to the QEPAS technique to recognize the contribution of gaseous components in a mixture, exhibiting absorption structures with a high overlap [93]. A multi-gas mixture containing methane, acetylene and nitrous oxide, in an N_2 matrix, was analyzed. The absorption spectra of these three gas species show a 97% overlap parameter [93]. A CW DFB-QCL having center emission wavelength at 7.719 μm was employed. Measurements were performed with a bare custom QTF with T-shaped prongs and a resonance frequency of about 12 kHz, in WM-*f* demodulation. A preliminary acquisition of each single-component reference spectrum was recorded, as reported in Fig. 12 (blue line, red line, green line). Then five mixtures were generated. As an example, the QEPAS spectrum measured for a mixture of 3000 ppm of methane, 350 ppm of acetylene and 350 ppm of nitrous oxide in N_2 is shown in Fig. 12 (black line). To perform PLS regression, a training set was created using the reference spectra. Data augmentation was obtained by linearly combining the reference spectra and adding normal distributed-noise.

By using PLSR analysis tool, the analytes concentrations were retrieved for all the five mixtures. The prediction errors were found to occur within the 2σ interval determined by the gas mixer uncertainty. A comparative analysis with the results obtained by using traditional multi-linear regression showed a decrease of the PLSR prediction error by a factor of about 5.

4.3. Widely tunable lasers for broadband detection

The spectral emission of the distributed-feedback quantum cascade lasers can be typically tuned by less than 20 cm^{-1} by thermally varying the refractive index via injected current or temperature tuning, the latter significantly affecting the output optical power [11]. Therefore, in gas spectroscopy, these lasers are usually employed to detect few-atom gas molecules, having narrow and resolved absorption lines. In the case of many-atom molecules, having broad absorption bands, external-cavity quantum cascade

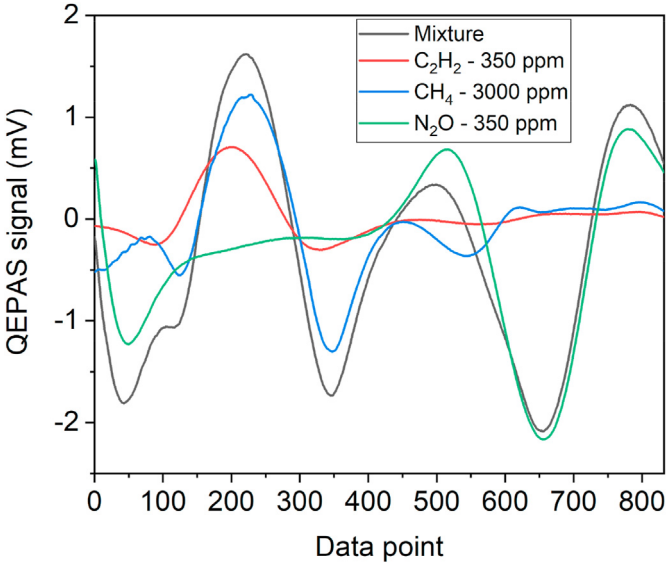

Fig. 12. 2f-QEPAS signal of the detected chemical species: three-gas mixture containing 3000 ppm of methane, 350 ppm of acetylene and 350 ppm of nitrous oxide, in nitrogen (black line); 1000 ppm of acetylene in nitrogen (red line); 3000 ppm of methane in nitrogen (blue line); 350 ppm of nitrous oxide in nitrogen (green line). (For interpretation of the references to colour in this figure legend, the reader is referred to the Web version of this article.)

lasers (EC-QCLs) with a mode-hop free/quasi-continuous frequency tuning are preferred due to a tuning range greater than 100 cm^{-1} [11].

In [94] R. Lewicki et al. used an EC-QCL to detect two broad absorption bands of pentafluoroethane in the range 1122 cm^{-1} - 1257 cm^{-1}. QEPAS measurements were performed by means of a standard spectrophone and implementing AM-*1f* demodulation. A preliminary measurement of the background signal was performed by flowing pure nitrogen through the sensor, to be then subtracted to the signal acquired for pentafluoroethane. In both cases, the laser power was acquired for each wavenumber and used to normalize the *X* and *Y* components of the QEPAS signal. Sensor calibration and MDL estimation were performed by mapping the *X* component of the background-subtracted pentafluoroethane QEPAS signal versus the absorption coefficient calculated from the reference spectrum, for each wavenumber. A linear sensor responsivity was confirmed, with a correlation coefficient R = 0.9989. A MDL of 4.5 ppb was obtained from the calibration slope [94]. To avoid the effects of the laser tuning instability and improve the MDL, the laser wavenumber was set at 1208.62 cm^{-1}, corresponding to the pentafluoroethane peak and the signal to noise ratio was calculated, leading to a MDL of about 3 ppb for a lock-in integration time of 1 s [94]. Furthermore, the use of a widely tunable EC-QCL to detect broadband absorbers having overlapped features has been demonstrated in Ref. [94] by targeting acetone and pentafluoroethane. The sensor was first calibrated for acetone detection by setting the wavenumber emission at 1217.7 cm^{-1}, in correspondence of the acetone absorption. The calculated MDL was ~ 520 ppb at a lock-in integration time of 1 s. However, the measured calibration coefficient was more than five times higher than the one measured for pentafluoroethane, meaning that these analytes relax energy through different pathways. Then, a mixture composed of pentafluoroethane and acetone in nitrogen was analyzed, and MLR was used to retrieve the two broadband absorbers' concentration.

In a similar experimental configuration, A. Kosterev et al. demonstrated the possibility to employ an EC-QCL as the light source of a QEPAS sensor for broadband absorbers detection in a rapid scan mode [95]. In fact, considering that the response time of the QTF can be calculated as $\tau = Q/\pi f_0$, a standard spectrophone with a quality factor of ~ 2000 provides a response time of ~ 20 ms, enabling thus a rapid sweep of the laser wavelength. In fact, the employed EC-QCL could be continuously tuned between 1196 cm^{-1} and 1281 cm^{-1} and the fastest scan (scan rate of 77.3 cm^{-1}/s) allowed the 85 cm^{-1}-wide tuning range to be swept in about 1.1 s. In this experiment, several standard QTF spectrophones were tested to select the most performant resonator. AM-*1f* demodulation was then implemented for analysis of gas mixture containing traces of pentafluoroethane, acetone, ethanol, and water. The experimental spectra were interpolated by a linear combination of reference spectra plus a frequency-dependent background signal. The analysis of the acquisition data point scatter was mainly focused on pentafluoroethane and acetone, retrieving a MDL of 13 ppb for a mixture of 15 ppm of pentafluoroethane in pure N_2 and of 250 ppb for a mixture of 200 ppm of acetone in pure N_2. Moreover, it was also verified that the precision in pentafluoroethane detection was substantially unaffected by the presence of ethanol vapor in the mixtures [95].

Recently, arrays of DFB-QCLs monolithically grown on a single semiconductor chip have been demonstrated. These devices represent an alternative to broadband emission, instead of EC-QCLs. Moreover, such laser sources are compact (as compared to EC-QCLs) and benefit from all the advantages of the DFB-QCLs [11]. In a recent work, Giglio et al. employed an array of pulsed DFB-QCL to develop a QEPAS sensor for detection of broadband absorber gases, characterized by overlapped features over a 150 cm^{-1}-wide spectral range [83]. Nitrous oxide and methane were selected as the target molecules, whose absorption features were analyzed in the 1190 cm^{-1} - 1340 cm^{-1} spectral range. The QCL array was operated in pulsed mode and measurements were performed in AM-1*f* demodulation. A custom spectrophone was employed, having an overtone resonance frequency of about 25 kHz. The QTF had a prong spacing of 1 mm to accommodate the slightly shifted beams coming out of the different devices. First, Giglio et al. proved the feasibility of broad detection of a N_2O in nitrogen [49]. Both temperature- and injected current-dependent wavelength tuning were exploited to acquire data points with a fine or coarse resolution of 0.27 cm^{-1} or ~4 cm^{-1}, respectively. Each spectrum was divided by the normalized optical power curve to take into account the output

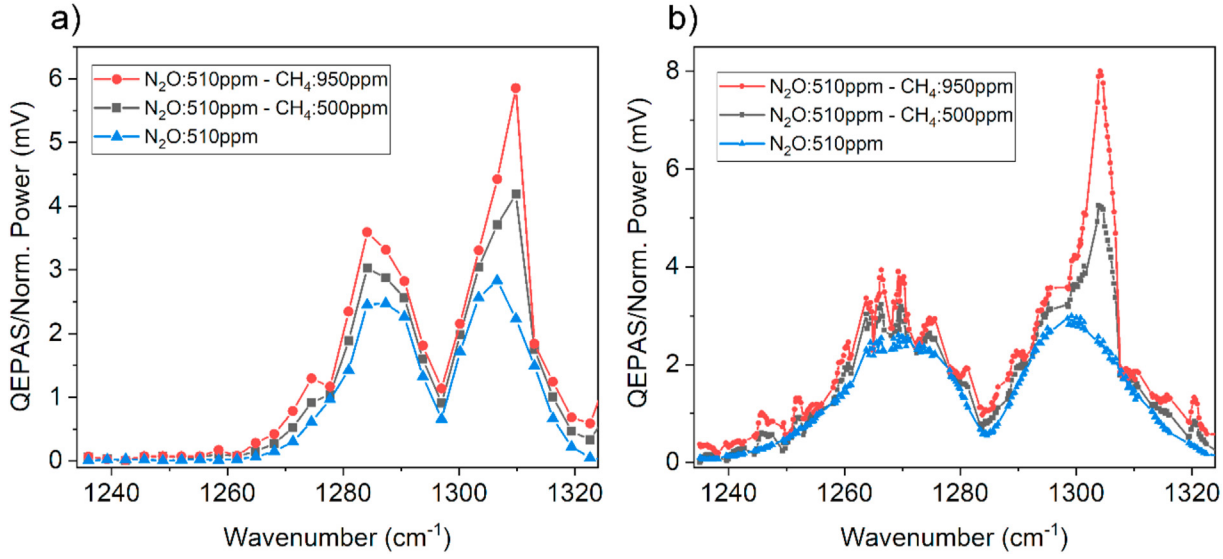

Fig. 13. a) Coarse resolution and b) fine resolution QEPAS spectra divided by the normalized optical power of a mixture of 510 ppm of N_2O in nitrogen (blue triangles), 510 ppm of N_2O and 500 ppm of CH_4 in nitrogen (black squares) and 510 ppm of N_2O and 950 ppm of CH_4 in nitrogen (red dots). (For interpretation of the references to colour in this figure legend, the reader is referred to the Web version of this article.)

power difference among the 32 devices. The obtained spectra well resembled the P- and R-branches of the absorption spectrum of nitrous oxide. The sensor linear responsivity with N_2O concentration was demonstrated by verifying the linear scaling of the area beneath the QEPAS spectrum. A MDL of 60 ppb was estimated for an integration time of 10 s, evaluated as the N_2O concentration corresponding to the area beneath the noise spectrum. The authors repeated the same measurements with methane, obtaining a well-reproduced envelope of the CH_4 absorption features, a linear responsivity of the sensor with CH_4 concentration and a MDL of about 200 ppb for the same integration time [83]. Then, multi-gas detection was demonstrated for broadband overlapping absorption features. With this aim, a reference spectrum for 510 ppm of N_2O in nitrogen (R_{510}^{N2O}) and for 1000 ppm of CH_4 in nitrogen (R_{1000}^{CH4}) were first acquired, both with fine and coarse spectral resolution. The two R_{510}^{N2O} are shown in Fig. 13 (blue triangles). Then, mixtures with 510 ppm of nitrous oxide and different concentrations of methane (150 ppm, 500 ppm and 950 ppm) in nitrogen, whose spectra are shown in Fig. 13 in the two acquisition modes, were generated.

Fig. 13 clearly shows how the nitrous oxide spectrum is affected by the presence of methane in the analyzed mixtures. In particular, CH_4 peaks at 1266.04 cm^{-1}, 1306.10 cm^{-1} and 1330.35 cm^{-1} emerge over R_{510}^{N2O} by increasing the CH_4 amount in the mixture, as shown in Fig. 13a. The overlap of the two spectra is even more clear by using a finer resolution (see Fig. 13b). The concentration of methane and nitrous oxide in the mixtures was calculated by using a traditional MLR approach to analyze the data acquired for both coarse and fine resolution. Equation (11) led to concentration values less than 6.5% and 5% discrepant with the nominal ones, in the two resolution approaches. Relative standard error was also calculated, resulting to be 6.2% for the mixture with 150 ppm of methane, due to hardly recognizable methane absorption features, and less than 3% for the other spectra acquired with coarse resolution. The relative standard errors on concentrations halved for spectra acquired with fine resolution, as it can be expected from a spectrum showing better reconstructed features [83]. In this review, we also report on a comparison with the results that can be achieved by analyzing the same data with a PLSR approach, as described in Section 4.2.2. Concentration values less than 6.8% and 4% discrepant with the nominal ones were obtained, for the coarse and fine resolution acquisition, respectively. For coarse resolution-acquired spectra, a relative standard error lower than 7% was found for the mixture with 150 ppm of methane, while it was below 2.2% for the other mixtures. In the case of spectra acquired with a fine resolution, the relative standard error was a factor 1.4 lower with respect to multi-linear regression. This comparison clearly shows the improved predictive capability of PLSR as compared with MLR.

5. Analysis of complex gas mixtures and fluctuating backgrounds

The detection of gaseous components in fluctuating backgrounds represents the major limit for photoacoustic techniques. Background fluctuations can arise from variations in concentration of different components of the gas matrix. This kind of variations mainly affect: i) the relaxation rate of the target molecule through the energy exchange channels with its collisional partners [23,29], ii) the interaction of the QTF with surrounding medium in terms of the resonance frequency shift and variation of the quality factor [13], iii) enhancement factor related to the micro-resonator tubes due to the variation of the sound speed [96]. Applications such as natural gas analysis at real concentrations require detection in a wide range of concentration. The evaluation of wetness and the balance requires the determination of the C1−C5 ratios which vary on the percent scale with consequent significant variation of the gaseous matrix [69,72,82]. The determination of the origins and temperature-induced effects on the formation of natural gas requires the evaluation of the isotopic ratios of the lightest alkanes such as methane, ethane and propane or other concerned non-hydrocarbons components such as H_2S [32]. More complete information can be gathered from the evaluation of isotopologues with extremely low natural abundance such as the deuterated methane $^{12}CH_3D$ and $^{13}CH_3D$ [97]. This is a matter of evaluating trace concentrations of the target molecule potentially in the ppb scale within backgrounds of variable components in the percent scale.

Environmental monitoring applications inherently have to deal with fluctuating backgrounds. The tracking of atmospheric concentrations of greenhouse gases, for determination and updating of global warming potentials as well as for identification and control of particulate and pollutant emissions, are normally carried out in several different air compositions. The QEPAS sensors demonstrated so far have implemented various strategies and adjustments essentially to eliminate the dependence on variations in water vapor concentration, which is known to act as a promoter for relatively slow relaxing molecules such as methane or carbon dioxide. In some cases, such as for the near-IR methane ethane sensor discussed in paragraph 4.2.1, the choice of the spectral range is functional to exclude a water vapor promoting effect when it varies in the range of percent. In other cases, such as the mid-IR sensor of atmospheric concentrations of CH_4 and N_2O reported in paragraph 3.2, a humidifier was used to enrich the analyzed air samples with water vapor in order to saturate the relaxation rate of the target molecules. This latter approach was adopted for QEPAS sensors devoted to breath analysis, where several biomarkers must be detected in traces within a large variety of exhaled breath compositions. In Table 1 are listed a selection of biomarkers with typical concentration ranges and related pathologies.

First implemented by Paulin et al., in 1971, breath analysis can be divided into two macro categories: off-line and on-line analysis. The off-line approach mainly consists in the analysis of exhaled breath contained in polymeric sample bags, which is the most common sampling method on an international scale.

Nevertheless, several real time breath analyzers based on gas-chromatography (GC) hyphenated methodologies, GC coupled with mass spectrometry, GC coupled with flame ionization detection, GC coupled with ion mobility spectrometry, have been demonstrated and still are under development. Real time breath analysis also includes all the techniques based on proton transfer reaction mass spectrometry, fast flow and flow-drift tube techniques called selected ion flow tube mass spectrometry [98] and a large number of electronic noses.

The laser-based techniques employed so far in breath sensing are tunable diode laser absorption spectroscopy, cavity ringdown spectroscopy, integrated cavity output spectroscopy, cavity enhanced absorption spectroscopy combined also with optical frequency comb lasers, cavity leak-out spectroscopy, photoacoustic spectroscopy and quartz-enhanced photoacoustic spectroscopy [99]. These real time approaches make all the operations related with sampling, storage and pre-concentration much easier. Furthermore, these quasi-real time techniques rely on sensitivity and selectivity levels comparable with mass spectrometry but exploiting potentially inexpensive point of care (POC) devices [99]. One of the most important advantages of these POC devices consists in their employment in mass screening, while the ability to simultaneously identify the broad chemical variation of the VOCs in exhaled breath has to be improved.

A QEPAS sensor for NH_3 trace detection in breath was developed at the Rice University in 2013 [100]. The detection sensitivity achieved was ~3 ppb of NH_3 at 1 s integration time, when targeting the

Table 1
Some representative biomarkers for the most important diseases.

Biomarker	Formula	Typical concentrations	Diseases
Carbon monoxide	CO	0.01–10 ppm	Asthma, angina, hyperbilirubinemia
Ammonia	NH_3	0–2 ppm	Stomach ulcers, Duodenal ulcers caused by helicobacter pylori, Liver disease
Nitric oxide	NO	10–50 ppb	Asthma, Chronic renal failure
Ethane	C_2H_6	0–10 ppb	Alzheimer disease, atherosclerosis, diabetes, cancer
Carbonyl sulfide	OCS	0–10 ppb	Liver disease, transplant rejection, Cystic fibrosis
Hydrogen cyanide	HCN	0–10 ppb	Cystic fibrosis
Isoprene	C_5H_8	0–100 ppb	Lung cancer, Cholesterol
Acetone	C_3H_6O	0–500 ppb	Lung cancer, Cardiovascular diseases, Diabates
Methanol	CH_4O	0–200 ppb	Lung cancer, Liver Chirrosis
Formaldehyde	CH_2O	0–10 ppb	Lung cancer
Hexanal	$C_6H_{12}O$	0–10 ppb	Breast cancer, Liver Cancer
Heptanal	$C_7H_{14}O$	0–10 ppb	Breast cancer, Lung cancer
Octanal	$C_8H_{16}O$	0–10 ppb	Breast cancer, Lung cancer
Nonanal	$C_9H_{18}O$	0–10 ppb	Breast cancer, Lung cancer
Pentane	C_5H_{12}	0–1 ppb	Cystic fibrosis, Lung cancer
Dimethyl sulphide	C_2H_6S	0–10 ppb	Cystic fibrosis, Lung cancer
2-Butanone	C_4H_8O	0–10 ppb	Liver cancer, Lung cancer
Trimethylamine	C_3H_9N	0–10 ppb	Liver cirrhosis
Acetaldehyde	C_2H_4O	0–50 ppb	Alcoholic hepatitis, Lung cancer

965.4 cm^{-1} line located in the ν_2 fundamental absorption band, by means of an EC-QCL and a standard spectrophone. To level out the water vapor influence a humidifier made from thin Nafion tubes was applied. Nevertheless, in some situations the spectral range of operation is mostly determined by the necessity of maximizing the cross-sections of the target molecules and avoiding potential interferences occurring from other gas components involved in a specific application (H_2O, CO_2, etc.). Thus, the dependence of relaxation dynamics on gas matrix fluctuations becomes a secondary issue. In some other situations, the addition of a specific device such as a humidifier may just not be suitable for the architecture of the detection apparatus. In this final chapter, some effective approaches to deal with the challenges given by the fluctuating backgrounds and make QEPAS a more robust and reliable technique will be discussed.

5.1. High concentration QEPAS measurements

Variations in the bulk composition of the carrier gas represents a major issue for several different applications in the gas sensing field. For example, this can happen in monitoring of hydrogen sulfide concentration in the gas diffusing through the fluid isolation layer of the flexible oil risers. The velocity of the corrosion process for the metal elements is mainly determined by the composition of the surrounding gas and by the H_2S concentration, whose effects become impactful at concentrations in the range 100–1000 ppm. The gas environment around the metal layers is formed by the gas species drifting from oil into the fluid isolation layer, typically CO_2 and CH_4, with concentrations that can vary within the two extremes $\sim$ 0%CH_4:100%CO_2 and $\sim$ 0% CO_2:100%CH_4. This specific application motivated A. Kosterev et al. to conduct a detailed composition analysis of a model gas mixture consisting of CO_2, CH_4 and trace amounts of H_2S [101]. All measurements were performed at atmospheric pressure, as required by the application. A QEPAS sensor based on two ADMs and two diode lasers was developed. The two ADMs mounted a standard bare QTF and a standard QTF spectrophone, respectively. Since the selected CO_2 and H_2S absorption bands overlap, one DFB diode laser emitting at $\lambda = 1.58$ μm was used for the detection of both species. A second DFB diode laser emitting at $\lambda = 1.65$ μm was employed to detect CH_4. The architecture of the sensor, equipped with a full system of single mode fibers for beam delivery and absorption cells for line-locked measurements, resembles the setups illustrated in Figs. 5 and 6. The use of a bare QTF served two purposes. The first one is the expansion of the dynamic range of the sensor ~10 times towards the high concentrations. Indeed, even if the linear dynamic range of the tuning fork itself is extremely wide and thus suitable for any practical gas sensing application, the dynamic range of the transimpedance amplifier and of the electronics for signal demodulation and analysis did not allow to measure both QTF thermal noise and QEPAS signals produced by a 100% CH_4 gas sample within the ADM mounting the spectrophone. Thereby, the bare QTF allowed expanding the dynamic range of ~10 times. The second reason consisted in providing a double check for an unambiguous interpretation of the experimental results. The detection sensitivity of the spectrophone was determined for each molecule, providing MDLs of 9.1 ppm, 123 ppm and 0.5 ppm for H_2S, CO_2 and CH_4 respectively, in humidified N_2-based mixtures [101]. The photoacoustic response of the sensor at high concentrations was evaluated for mixtures containing 0.5% H_2S and variable amounts of CH_4 and CO_2. The weak H_2S signal, caused by the relatively low linestrength combined with the trace concentration scale, required the only use of the standard QTF spectrophone for H_2S measurements. Since methane concentrations caused the $S(CH_4)$ signal from the spectrophone to saturate the electronics, only the bare QTF was used for the CH_4 measurements. For carbon dioxide, where the weak $3\nu_3 + \nu_1$ targeted band was compensated by a high concentration level, $S(CO_2)$ signals from both spectrophones were acquired. Resonance frequency, quality factor Q and detection phases, both for the QTF and the spectrophone, were investigated for each analyte. It was found that CH_4 acts as V-T relaxation catalyst just like H_2O in N_2. Thus, in gas mixtures containing > 5% CH_4, relaxation of both CO_2 and CH_4 is fast enough to satisfy $2\pi f\tau < 1$ condition and the QEPAS signal measured is not significantly affected by the energy relaxation process. Carbon dioxide, however, was demonstrated to have an impact on the V-T relaxation of H_2S, branching part of the initial excitation into slowly relaxing intramolecular states and thus this portion of energy did not contribute to the photoacoustic signal. Furthermore, the H_2S signal measured from the spectrophone is mainly influenced by variations of sound speed at different CH_4–CO_2 concentrations. This led the authors to avoid the evaluation of the enhancement factor related to the acoustic resonators and adopt a more pragmatic data analysis procedure consisting of three steps: i) use $S(CO_2)/Q$ data from the bare QTF to determine the concentration of CO_2 through the calibration curve; ii) use the CO_2 concentration to select the branch on the CH_4

calibration curve, which is not an injective function of methane concentration and shows a maximum at 54% (CO_2 at 46%), and thus determine the CH_4 concentration using $S(CH_4)/Q$ data from the bare QTF; iii) use $S(CO_2)$ data from spectrophone as the spectrophone sensitivity calibration. This approach avoid the user to continuously characterize the AR's resonance curve, whose shift depends on the gas composition and temperature, and allow retrieving the H_2S concentration from the spectrophone signal and the H_2S vs CO_2 calibration curve [101]. This sophisticated approach is however limited by the possibility that the carrier gas may contain several percent quantities of other gas species besides CO_2 and CH_4, resulting in an accuracy reduction of the concentrations retrieved because of the change of the sound speed. A similar scenario can be found in natural gas analysis, when the concentrations of each component are normally measured in the percent scale.

A QEPAS sensor for methane, ethane and propane trace gas detection demonstrated by A. Sampaolo et al. was already discussed in paragraph 4.2.1. A further work by G. Menduni et al. [102] {FormattingCitation} took on the challenge of high concentration mixtures of hydrocarbons, composed of methane (C1) and ethane (C2) and employing the same ICL in a similar QEPAS sensor architecture. In this study, 1:10 dilutions in nitrogen (N_2) of natural gas-like mixtures were analyzed by using a compact gas mixer upstream the sensor. An example of gas mixtures QEPAS spectra is reported in Fig. 14a. Two partially-merged C1 absorption features can be observed corresponding to a laser injection current I_{laser} = 52 mA and I_{laser} = 54 mA, while two well-separated C2 absorption features can be observed at I_{laser} = 43 mA and I_{laser} = 69 mA. Significant variations of the C1 peak signal in particular were observed changing the samples composition. As an example, the QEPAS peak values for a fixed concentration of C1 with varying C2 is reported in Fig. 14b.

C1 peak signals are significantly higher when C2 is introduced in the gas matrix compared to the one acquired a in pure nitrogen matrix. Moreover, C1 peak values vs C2 concentration changes do not show a monotonic trend. The sharp increase in C1 signal, from the one obtained in pure N_2 to the one recorded when 1000 ppm of C2 are added to the mixture, is due to the modification of the density of energy levels available for V-T relaxation. Once reached a C1 signal plateau from 2000 ppm to 6000 ppm of C2, the signal starts decreasing because of the quality factor deterioration and the sound speed variation.

In order to analyze the acquired QEPAS mixtures spectra and retrieve concentrations of the analytes, PLSR analysis was used. As already discussed in paragraph 4.2, this statistical method has proven its potential with highly-overlapping QEPAS spectra [93] and it is a well-established approach in different spectroscopic fields for its capability of dealing with matrix effects [103,104].

The PLSR was set implementing a machine learning approach, with a calibration step and a test step. The measurement dataset was split assigning 36 spectra to the calibration set and 4 spectra to the test set, whose compositions were unknown to the regression algorithm. The test measurements were selected among those characterized by a composition similar to natural gas samples from real-field applications (C1 > 7%, C2 ≈ 0.2%–0.8%, considering the 1:10 dilution in N_2). The number of PLS components to be used for the analysis was determined by means of a validation step using a 10-fold cross-validation method. The optimal number of components was evaluated using the root mean square error of cross-validation (RMSECV) as selecting parameter and it was found equal to three. Following this preliminary step, the calibration of the PLS algorithm was performed and the regression coefficients matrix was calculated. Using these calibration model, the concentrations of the hydrocarbons in the test set were predicted and compared to the expected ones, as shown in Fig. 15a and b for C1 and C2, respectively. In Table 2 are reported the retrieved concentrations.

The calibration data of both chemical species were linearly fitted and the returned determination coefficient R^2 was equal to 0.997 for C1 and 0.990 for C2. The root mean square error of calibration (RMSEC) was used to evaluate the PLSR model and was equal to 0.23% and 0.029% for C1 and C2, respectively. The root mean square error of prediction (RMSEP) for the test samples was used to quantify the prediction capabilities of the PLSR models and was found equal to 0.26% and 0.028% for C1 and C2, respectively. The achieved results confirm the ability of the employed statistical method to retrieve gas sample compositions with a good accuracy, leveling out or at least reducing the impact of gas matrix variations on photoacoustic generation and detection.

An alternative approach for the characterization of high concentration absorption backgrounds was developed by M. Mordmueller et al. for bio-gas analysis applications [105]. In this detection scheme, sequential photoacoustic and electric excitation of the QTF allows discriminating the influences of the background gas and the target analytes. The separation of the two effects is due to the fact that the electrically induced oscillation amplitude is directly related to the damping from the surrounding medium, while the signal amplitude, related to the photoacoustic excitation,

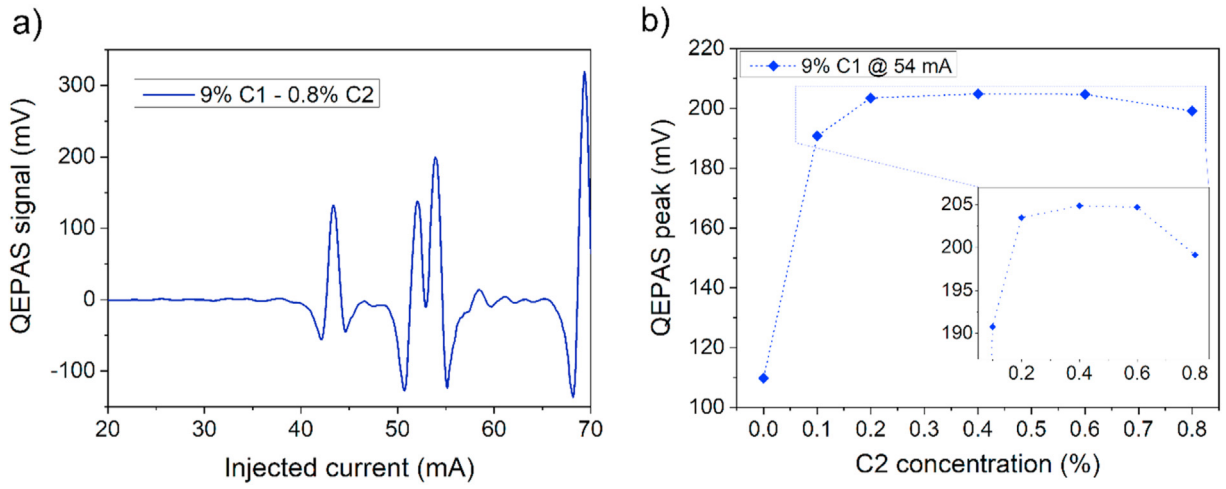

Fig. 14. a) QEPAS spectrum of the mixture composed of 9% C1, 0.8% C2 and N_2. b) QEPAS peak signals of a fixed 9% C1 concentration with varying C2 in nitrogen.

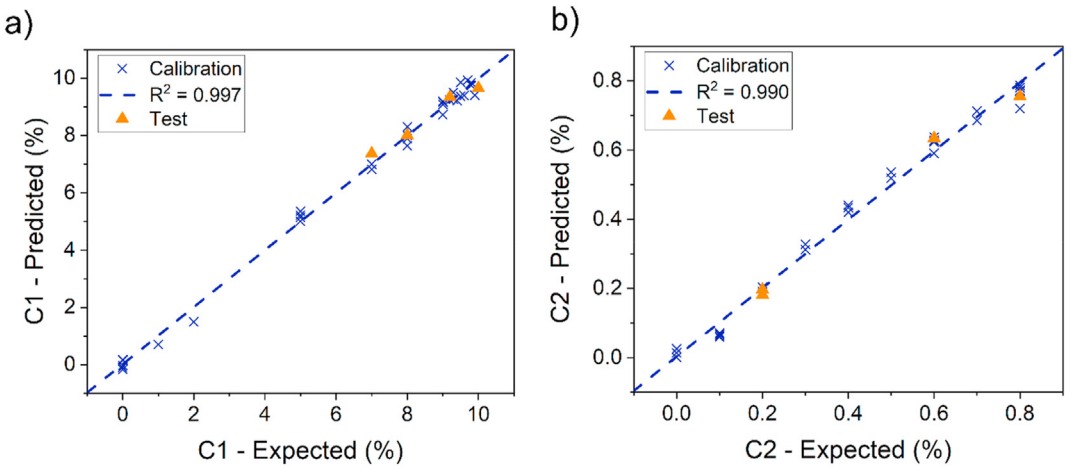

Fig. 15. Plot of predicted concentrations versus expected concentrations of a) C1 and b) C2. Both the test set (orange triangles) and the calibration set (blue crosses) are shown, alongside with the linear fit of the calibration data set (dashed line). (For interpretation of the references to colour in this figure legend, the reader is referred to the Web version of this article.)

Table 2
Comparison between expected concentrations and PLSR-predicted concentrations for the test set.

	Expected (%)		Predicted (%)	
mixture	C1	C2	C1	C2
#1	7.0	0.20	7.4	0.20
#2	8.0	0.60	8.0	0.63
#3	9.2	0.80	9.3	0.76
#4	10.0	0.20	9.7	0.18

is also depending on the target gas concentration. This approach was implemented and tested using a mixture of the target gas methane with oxygen, acting as relaxation energy sink and thus as a retarder, and with helium which on the other hand acts as a relaxation promoter. The amplitude induced by electrical excitation and the fading time were analyzed instead of photoacoustic amplitude. As a result, a MDL comparable with the standard QEPAS configuration was demonstrated.

The additional benefit of the electric driving consists in the fact that a variation in the generated amplitude implies a variation of the damping conditions in the surrounding gas. This property can either be exploited as a trigger for recalibration, i.e., determination of the actual resonance frequency. In alternative, it can be used combined with an auto-trigger ensuring the permanent locking to the current resonance frequency of the tuning fork. In this way, the damping parameters associated with the gas matrix in which the resonator is immersed can be extracted from the data avoiding the determination of the QTF's resonance frequency or Q-factor [106].

The necessity of tracking the QTF resonance frequency, while the gas and operating conditions are changing, stimulated the implementation of several diverse spectroscopic configurations. The Beat Frequency QEPAS (BF-QEPAS) was conceived by H. Wu et al., in 2017 and allows the continuous monitoring of the frequency and Q-factor of the QTF, together with the trace-gas concentration. This technique is based on the analysis of the beat frequency signal generated when the transient response signal of the QTF is demodulated at its non-resonance frequency [107].

The BF-QEPAS approach was successfully employed by Rousseau et al. for monitoring the influence of temperature and humidity variations in gas mixtures on QEPAS detection. In this configuration, the QTF characterization was implemented in a feedback loop in order to pursue the resonance tracking of the QTF (RT-QEPAS). RT-QEPAS provided a consistent reduction of the signal drift, less than 1% relative error compared to 44% for conventional QEPAS [108].

With the same aim of enabling fast and precise QEPAS measurements, Levy et al. introduced a novel signal processing technique based on a closed loop detection scheme and alternative to the traditional open loop lock-in detection. In this processing scheme the QTF is actuated at resonance by means of an oscillator circuit; the oscillator output signal is quadrature phase-shifted and used to modulate the laser intensity. This induces a shift of the oscillator frequency that is proportional to the photoacoustic force and thus to the gas concentration, allowing instantaneous concentration measurements [109].

5.2. *Self-calibrating dual gas QEPAS sensors*

Simultaneous detection and discrimination of different absorbers in a gas mixture is normally a request for many applications fields, such as monitoring of isotope ratios or diagnostic of breath samples for measuring a set of biomarkers at the same time. The multi-gas detection discussed so far is implemented by scanning the laser current and exploits the spectral tuning range of the laser device or, as alternative, by sequentially locking the laser emission to different absorption peaks related to specific absorbing molecules.

In this case, the measurements of multiple analytes' concentration is not simultaneous since a certain time is needed to drive the laser source through the tuning scan or through a discrete sequence of different emission wavelengths. Thereby, the only effective approach to carry out an actual simultaneous detection of different gas species consists in multiplexing several independently operated laser sources, all of them combined with a single detector, by employing a frequency-modulated multiplexing scheme.

The above mentioned detection scheme cannot be easily implemented in spectroscopic systems based on multi-pass or high finesse optical cavities approaches because of the complexity of the sensing architectures and the limited operability of the optical elements over a wide spectral range. Instead, for QEPAS, the fundamental and overtone combined vibration described in paragraph 2.5.2, can be effectively implemented to achieve simultaneous dual gas detection and, for example, allow a real-time compensation of water vapor relaxation promoting effect on detection of environmental molecules [38].

H. Wu et al., in 2019 reported on a QEPAS methane sensor for atmospheric CH_4 detection near a landfill based on a V-T relaxation self-calibration approach [56]. With the aim of normalizing the impact of water vapor on the energy relaxation rate of methane molecules, H_2O and CH_4 concentrations were simultaneously detected by exciting the first overtone and the fundamental mode of a custom QTF, having a resonance frequency at 17.7 kHz and 2.8 kHz, respectively. At the overtone lower antinode, a single tube resonator was applied to enhance the QEPAS response at the CH_4 photoacoustic excitation. A CW DFB-ICL operating at 3.3 μm and a near-IR DFB laser diode emitting at 1.37 μm were used to photoacoustically excite methane and water vapor molecules, respectively.

For methane detection, the anti-symmetric stretching vibration ν_3 band located at 3038.5 cm^{-1} was targeted. When humidified N_2 is employed as carrier gas, the CH_4 V-T relaxation process can be modeled considering a simplified scheme in which only a one-stage molecules collision is taken into account [110]. Thereby, the *2f*-QEPAS signal amplitude $S(P_H)$ measured for methane can be also calculated using Eq (12).

$$S(P_H) = S_1 + S_2 = S_1 \left[1 + \left(\frac{S_\infty}{S_0} - 1 \right) \Big/ \sqrt{1 + \frac{(2\pi \cdot f \cdot \tau_0^H \cdot P_0)^2}{P_H^2}} \right] \tag{12}$$

where S_0 and S_∞ are the CH_4 signals measured in a dry N_2–based mixture and or in saturated water pressure conditions, respectively. S_1 is the signal arising from the CH_4/N_2 collisions and it doesn't depend on the water vapor concentration, while S_2 is the contribution to the CH_4 signal arising from energy relaxation through the CH_4/H_2O collisions, whose rate depends on the H_2O partial pressure P_H. The self-relaxation through CH_4/CH_4 collisions can be assumed negligible because of the trace concentration scale (hundreds of ppm) of CH_4. $\tau_0^H \mathrm{n} P_0$ is the time constant characterizing the V-T relaxation process due to CH_4/H_2O collisions. Being the modulation frequency f is usually $>10^4$ Hz for QEPAS,for low values of H_2O partial pressure P_H, Eq. (12) can be re-written as a linear equation:

$$S(P_H) \approx S_1 + \left(\frac{S_\infty}{S_0} - 1 \right) \cdot \frac{S_1}{2\pi \cdot f \cdot \tau_0^H \cdot P_0} \cdot P_H \tag{13}$$

The slope k of $S(P_H)$ is:

$$k = \left(\frac{S_\infty}{S_0} - 1 \right) \cdot \frac{S_1}{2\pi \cdot f \cdot \tau_0^H \cdot P_0} \tag{14}$$

After the value $\tau_0^H \cdot P_0$ is calculated through the measured slope k, S_1 can be written as a simple function of $S(P_H)$ and P_H. Thus, the influence of H_2O on the V-T energy relaxation of the excited methane molecules can be calibrated and the real CH_4 concentration can be extracted, once P_H and $S(P_H)$ are simultaneously measured, demodulating the QTF signal at fundamental and first overtone resonance frequencies, respectively.

The first overtone detection channel output at different CH_4 concentrations (from 50 ppm to 500 ppm) with a selected H_2O concentration at 1.6%, was first demonstrated. A linear behavior was also verified for H_2O concentration through the fundamental detection channel. Then, the experimental curve of CH_4 QEPAS signal at a fixed concentration (500 ppm) as a function of H_2O concentration in the mixtures (from 0% to 1.6%) was obtained. The curve was linearly fitted as a function of P_H and the slope value extracted was $k = 0.00248$, leading to the following formula for methane signal compensation with respect to the water vapor content of the mixture:

$$S_1 = \frac{S(P_H)}{1 + 0.9934 \cdot P_H} \tag{15}$$

With the aim of evaluating the self-calibration performance of the dual gas QEPAS sensor, a certified mixture of 500ppm-CH_4:N_2 and water vapor was flushed trough the ADM. The H_2O concentration was progressively varied.

The QEPAS signals related to methane $S(P_H)$ (black lines) and the QEPAS signals related to the water vapor partial pressure P_H (black lines) were acquired and plotted as a function of time (Fig. 16). The compensated CH_4 QEPAS signals S_1 (red line), calculated from Eq. (15) are also plotted in Fig. 16. The stability of S_1 values demonstrated how effective is the normalization of the CH_4 detection with respect to the water concentration for this dual gas QEPAS sensor. The MDL at 1 s integration time resulted 32 ppm for H_2O and 50 ppb for CH_4, respectively [56].

The sensor was then tested nearby the Hou Village Landfill (HVL) in the Shanxi province, China, with the aim of monitoring methane environmental levels. The self-calibrating sensor was installed in a van, while an AC inverter was used to provide electrical power to the sensor using the car battery. The full data analysis, including the real-time methane signal compensation, was carried out by a custom LabVIEW-based program. The updating rate of the program for data acquisition was set to 10 s and all the measurements were performed for 3 h. Experimental results are shown in Fig. 17.

The average concentration of environmental methane nearby the HVL was ~2.9 ppm, which is > 1.5 times higher with respect to the expected average concentration in atmosphere (1.8 ppm). The observed three CH_4 peaks of ~4.1 ppm, 4.3 ppm and 5.9 ppm were detected by the sensor because of the wind blowing along the direction of the collection and sampling system. The pseudo-periodic sharp peaks, delayed from each other by ~45 min, were correlated to solid waste trucks passing nearby the CH_4 sensor [56].

A dual-gas QEPAS sensor for simultaneous detection of H_2O and alternatively CH_4 or N_2O was also demonstrated by A. Elefante et al. [55]. A QCL and a diode laser were employed to independently and simultaneously excite both the first overtone and the fundamental flexural mode, respectively, of a custom QTF. The diode laser wavelength emission was resonant with a H_2O absorption line

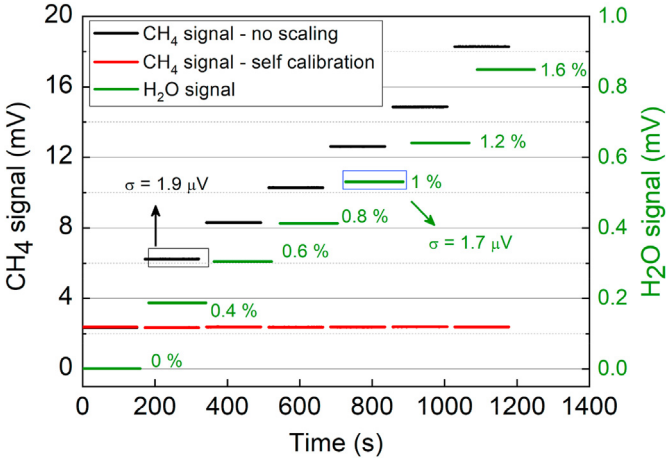

Fig. 16. Methane QEPAS signals (black lines) measured as a function of time, while varying in steps the water vapor concentration. Water vapor QEPAS signals (green lines) as a function of time. The red lines represent S_1 values calculated from Eq. (15). (For interpretation of the references to colour in this figure legend, the reader is referred to the Web version of this article.)

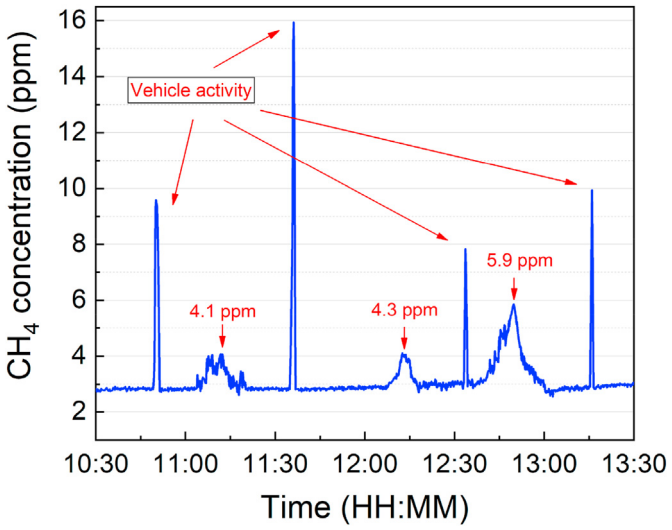

Fig. 17. Real time in-situ measurement of atmospheric methane nearby the Hou Village Landfill, Taiyuan, China on Oct. 11, 2018.

falling at 7181.16 cm^{-1} (1.392 μm), while the QCL, emitting at 7.71 μm, was tuned to excite two absorption features of N_2O and CH_4, falling at 1297.05 cm^{-1} and 1297.47, respectively.

In this sensor, the custom QTF employed is the same implemented in the dual-gas sensor demonstrated by Wu et al. [56], with the difference that in this case two different AR systems were aligned in on-beam configuration in correspondence of antinode points of the fundamental and the first overtone mode, respectively, to amplify the QEPAS SNR (Fig. 18).

The MDLs achieved at a lock-in integration time of 100 ms for methane, nitrous oxide and water vapor were calculated as low as 18 ppb, 5 ppb and 20 ppm, respectively.

This sensor prototype opens up interesting prospects for the use of quantum cascade lasers aligned to the fundamental mode antinode and lower antinode of the overtone. In fact, the high detection sensitivity guaranteed for both demodulation frequencies set the basis for applications in which a sequential and/or simultaneous multi-gas detection approach can be implemented and assisted by multivariate analysis. One of the most immediate field of application would be trace detection of heavy hydrocarbon molecules by performing real time signal compensation with respect to a methane-based gas matrix. A similar scenario would be the evaluation of isotope ratios by normalizing the photoacoustic response of the less abundant isotope with respect to the concentration of the more abundant one.

Finally, by fully exploiting the wavelength independence of the QTF sound detection, multi-gas analyzers implementing fiber-

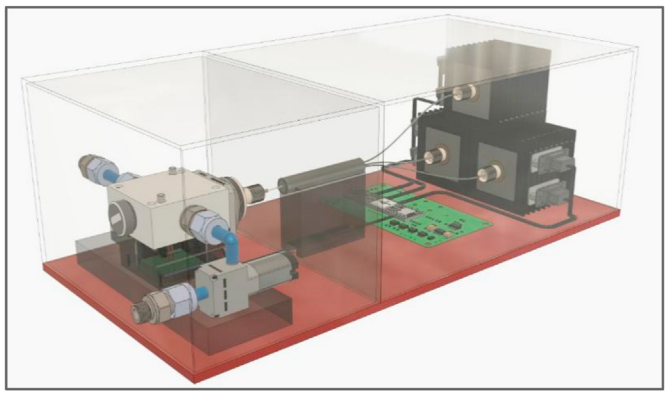

Fig. 19. Schematic of a QEPAS multi-laser gas analyzer. The laser module could be exchanged with different modules supporting alternate wavelengths and coupling methods.

combined multiple radiation sources (for example ICLs and/or QCLs) and smart modular sensing systems can be designed and developed. These systems, in which the lasers can be easily switched while keeping fixed the remaining parts of the sensor, represent the natural evolution of QEPAS sensing. A possible schematic of a multi-laser gas analyzer is shown in Fig. 19.

6. Conclusions

Multi-gas optical detection represents nowadays a spectroscopic approach allowing a comprehensive and systematic characterization of a specific gaseous mixture [111]. The information that can be retrieved from this kind of analysis becomes extremely useful for all the science fields in which the monitoring, prevention and diagnostics phase is of fundamental importance [4]. For example, the identification, tracking and quantification of biomarkers allows a prompt diagnosis of infections and carcinogenesis by means of breath analysis [2,112]. The mapping of natural gas composition in petroleum exploration enables: i) the reconstruction of the origin and evolution of natural gas reservoir; ii) production estimation; iii) early identification of dry wells to stop drilling, save time and money and significantly reduce the environmental impact [69,82]. Environmental monitoring of greenhouse gases' atmospheric concentrations allows the evaluation of their impact in terms of global warming potentials, as well as the identification of anomalous concentrations of certain molecules that are symptomatic of the onset of wildfires, or toxic gases' leakage and diffusion [3,63,83].

The main merits of spectroscopic techniques based on laser sources are the high selectivity and sensitivity, with the possibility

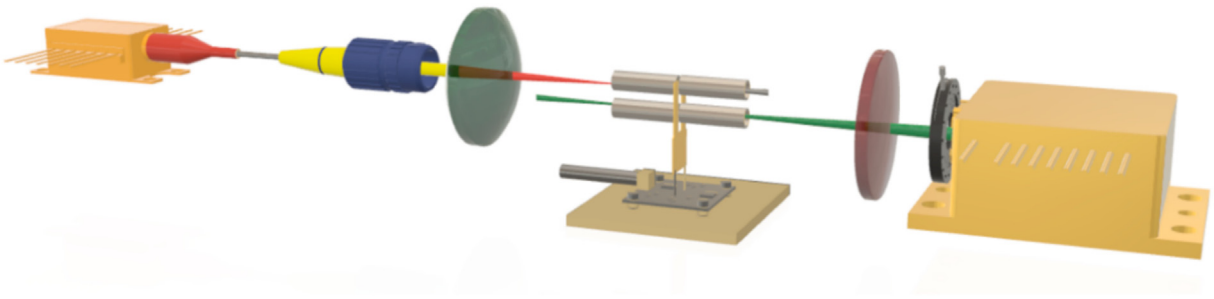

Fig. 18. Schematic of a dual-gas configuration employing a QCL aligned through a pair of ARs at the lower antinode of the first overtone mode, and a laser diode aligned through a pair of ARs at the antinode of the fundamental mode.

of pursuing a fairly good level of sensor compaction, depending on the spectroscopic technique selected and its specific detection apparatus [4]. Quartz-enhanced photoacoustic spectroscopy represents a smart solution mainly because i) the use of optical detectors, which cost in the same order of magnitude as the laser sources, can be avoided; ii) swapping the laser source is very easy thanks to the modularity of the detection apparatus, iii) the implementation of multiple laser sources and multiple acoustic resonators in a single QEPAS sensor is possible without excessively complicating the setup architecture [13,14].

In fact, other techniques relying on direct absorption must necessarily employ an optical detector, introducing thus a further weight, cost and power consumption. For TDLAS-based techniques the price to pay for high sensitivity is a fairly large light-gas interaction pathlength, which generally results in an increased sampling volume and increased weight of the multi-pass cell. In CEAS-based sensors, high-finesse cavities require high reflection mirrors, which cost is also comparable with the laser source and the narrow spectral bandwidth provided by the high reflection coatings makes this approach not suitable for wide wavelength tuning detection.

The fundamental purpose of this review is bringing to the reader's attention the advantages that could be gained in using the QEPAS technique for multi-gas detection, as well as discussing the possible issues deriving from its implementation and the strategies to reduce their impact on detection performances.

In the second chapter, the characteristics of standard, custom quartz tuning forks and spectrophones are summarized, with particular focus on their capability to work in harsh environments and adapt to the characteristics of the laser sources and different gas sample compositions [26]. In particular, the introduction of custom resonators from 2013 to date has allowed the development of innovative QEPAS approaches such as dual-gas simultaneous detection [38].

In the third chapter, QEPAS in its most suited application is discussed: multi-gas detection of trace gases by exploiting non-interfering absorption features. The use of laser diodes in particular enables the incorporation of up to four laser sources and four spectrophones within the same sensor [61]. Under the conditions of zero cross-talk among absorption lines and in the presence of gaseous traces within a fixed matrix, evaluations of isotope ratio variations were also demonstrated with remarkable accuracy and precision [69–71].

In the fourth chapter, multi-gas QEPAS sensors with interfering absorption bands are presented and discussed. The insensitivity of the acoustic resonator to the excitation wavelength enables the implementation of laser sources with large tunability, such as EC-QCL or laser arrays [83,95]. When the spectral characteristics of the target molecules are strongly overlapped, the study of the detection phase to discriminate different absorbers is fundamental and multivariate analysis techniques are exploited [75]. In particular, Multi-Linear Regression and Partial Least Square Regression statistical approaches are discussed [93].

Finally, in the fifth chapter the fundamental physical issue affecting photoacoustic techniques is discussed: gas detection in fluctuating backgrounds. To minimize the effects of the gas matrix on detection accuracy and precision, some possible solutions have been presented, such as: i) simultaneous use of a bare tuning fork and a spectrophone to evaluate in sequential steps the variation of the matrix and the adaptation of the calibration curves [101]; ii) use of PLSR in combination with a large data set to filter out the matrix variation effects on the detection of individual components [102]; iii) implementation of self-calibrating sensors for real time compensation of QEPAS signals with respect to the concentration of relaxation promoters [55,56].

Further developments of the QEPAS technique applied to multi-gas detection are based on the design, production and implementation of custom resonators, capable of better matching the spatial characteristics and power distribution of the laser sources, as well as the relaxation dynamics of the gas samples to be analyzed [113].

Integrated optics approaches for the design and development of lab-on-chip QEPAS sensors, including wafer bonded lasers sources, beam delivery waveguides and monolithically grown acoustic resonators, pave the way to complex, robust and ready-to-deploy multi-gas QEPAS sensor systems for real time and in-situ detection [114].

Declaration of competing interest

The authors declare that they have no known competing financial interests or personal relationships that could have appeared to influence the work reported in this paper.

Acknowledgments

The authors from Dipartimento Interateneo di Fisica di Bari acknowledge financial support from the European Union's Horizon 2020 research and innovation programme via the Marie Skłodowska-Curie project OPTAPHI, grant No. 860808 and THORLABS GmbH within the PolySenSe joint-research laboratory. The authors from Shanxi University acknowledge financial support by the National Natural Science Foundation of China (Grant Nos. 61805132) and 111 project (D18001).

Appendix A. Supplementary data

Supplementary data to this article can be found online at https://doi.org/10.1016/j.aca.2021.338894.

References

[1] M.H. Saberi, A.R. Rabbani, Origin of natural gases in the permo-Triassic reservoirs of the coastal fars and Iranian sector of the Persian Gulf, J. Nat. Gas Sci. Eng. 26 (2015) 558–569, https://doi.org/10.1016/j.jngse.2015.06.045.
[2] J. Pereira, P. Porto-Figueira, C. Cavaco, K. Taunk, S. Rapole, R. Dhakne, H. Nagarajaram, J.S. Câmara, Breath analysis as a potential and non-invasive frontier in disease diagnosis: an overview, Metabolites 5 (2015) 3–55, https://doi.org/10.3390/metabo5010003.
[3] C.B. Schmidt Dubeux, E.L. La Rovere, Local perspectives in the control of greenhouse gas emissions - the case of Rio de Janeiro, Cities 24 (2007) 353–364, https://doi.org/10.1016/j.cities.2007.01.012.
[4] J. Hodgkinson, R.P. Tatam, Optical gas sensing: a review, Meas. Sci. Technol. 24 (2013), https://doi.org/10.1088/0957-0233/24/1/012004.
[5] X. Liu, S. Cheng, H. Liu, S. Hu, D. Zhang, H. Ning, A survey on gas sensing technology, Sensors 12 (2012) 9635–9665, https://doi.org/10.3390/s120709635.
[6] D. Kohl, Function and applications of gas sensors, J. Phys. D Appl. Phys. 34 (2001), https://doi.org/10.1088/0022-3727/34/19/201.
[7] S. Neethirajan, D.S. Jayas, S. Sadistap, Carbon dioxide (CO_2) sensors for the agri-food industry-A review, Food Bioprocess Technol. 2 (2009) 115–121, https://doi.org/10.1007/s11947-008-0154-y.
[8] M.H. Chang, D. Das, P.V. Varde, M. Pecht, Light emitting diodes reliability review, Microelectron. Reliab. 52 (2012) 762–782, https://doi.org/10.1016/j.microrel.2011.07.063.
[9] P.A. Martin, Near-infrared diode laser spectroscopy in chemical process and environmental air monitoring, Chem. Soc. Rev. 31 (2002) 201–210, https://doi.org/10.1039/b003936p.
[10] J.R. Meyer, W.W. Bewley, C.L. Canedy, C.S. Kim, M. Kim, C.D. Merritt, I. Vurgaftman, The interband cascade laser, Photonics 7 (2020), https://doi.org/10.3390/PHOTONICS7030075.
[11] M.S. Vitiello, G. Scalari, B. Williams, P. De Natale, Quantum cascade lasers: 20 years of challenges, Opt Express 23 (2015) 5167, https://doi.org/10.1364/oe.23.005167.
[12] B. Mroziewicz, External cavity wavelength tunable semiconductor lasers - a review, Opto-Electron. Rev. 16 (2008) 347–366, https://doi.org/10.2478/s11772-008-0045-9.
[13] P. Patimisco, G. Scamarcio, F.K. Tittel, V. Spagnolo, Quartz-enhanced photoacoustic spectroscopy: a review,, Sensors 14 (2014) 6165–6206, https://doi.org/10.3390/s140406165.

[14] P. Patimisco, A. Sampaolo, L. Dong, F.K. Tittel, V. Spagnolo, Recent advances in quartz enhanced photoacoustic sensing, Appl. Phys. Rev. 5 (2018), https://doi.org/10.1063/1.5013612.
[15] L. Dong, F.K. Tittel, C. Li, N.P. Sanchez, H. Wu, C. Zheng, Y. Yu, A. Sampaolo, R.J. Griffin, Compact TDLAS based sensor design using interband cascade lasers for mid-IR trace gas sensing, Opt Express 24 (2016) A528, https://doi.org/10.1364/oe.24.00a528.
[16] Z. Wang, P. Fu, X. Chao, Laser absorption sensing Systems : challenges, Appl. Sci. 9 (2019) 2723–2750.
[17] I. Galli, S. Bartalini, S. Borri, P. Cancio, D. Mazzotti, P. De Natale, G. Giusfredi, Molecular gas sensing below parts per trillion: radiocarbon-dioxide optical detection, Phys. Rev. Lett. 107 (2011) 1–4, https://doi.org/10.1103/PhysRevLett.107.270802.
[18] G. Gagliardi, H.-P. Loock, A. Adibi, H. Weber, W.T. Rhodes, Cavity-enhanced spectroscopy and sensing. https://doi.org/10.1007/978-3-642-40003-2, 2014.
[19] A. Elia, P.M. Lugarà, C. di Franco, V. Spagnolo, Photoacoustic techniques for trace gas sensing based on semiconductor laser sources, Sensors 9 (2009) 9616–9628, https://doi.org/10.3390/s91209616.
[20] A.A. Kosterev, Y.A. Bakhirkin, R.F. Curl, F.K. Tittel, Quartz-enhanced photoacoustic spectroscopy, Opt. Lett. 27 (2002) 1902, https://doi.org/10.1364/OL.27.001902.
[21] P. Patimisco, A. Sampaolo, Y. Bidaux, A. Bismuto, M. Scott, J. Jiang, A. Muller, J. Faist, F.K. Tittel, V. Spagnolo, Purely wavelength- and amplitude-modulated quartz-enhanced photoacoustic spectroscopy, Opt Express 24 (2016), https://doi.org/10.1364/OE.24.025943.
[22] A. Miklós, Acoustic Aspects of Photoacoustic Signal Generation and Detection in Gases, Springer, US, 2015, https://doi.org/10.1007/s10765-015-1875-6.
[23] A.A. Kosterev, Y.A. Bakhirkin, F.K. Tittel, S. McWhorter, B. Ashcraft, QEPAS methane sensor performance for humidified gases, Appl. Phys. B Laser Opt. 92 (2008) 103–109, https://doi.org/10.1007/s00340-008-3056-9.
[24] P. Patimisco, A. Sampaolo, M. Giglio, S. Dello Russo, V. Mackowiak, H. Rossmadl, A. Cable, F.K. Tittel, V. Spagnolo, Tuning forks with optimized geometries for quartz-enhanced photoacoustic spectroscopy, Opt Express 27 (2019) 1401, https://doi.org/10.1364/oe.27.001401.
[25] P. Patimisco, A. Sampaolo, L. Dong, M. Giglio, G. Scamarcio, F.K. Tittel, V. Spagnolo, Analysis of the electro-elastic properties of custom quartz tuning forks for optoacoustic gas sensing, Sensor. Actuator. B Chem. 227 (2016) 539–546, https://doi.org/10.1016/j.snb.2015.12.096.
[26] P. Patimisco, A. Sampaolo, H. Zheng, L. Dong, F.K. Tittel, V. Spagnolo, Quartz–enhanced photoacoustic spectrophones exploiting custom tuning forks: a review, Adv. Phys. X 2 (2017) 169–187, https://doi.org/10.1080/23746149.2016.1271285.
[27] V. Spagnolo, P. Patimisco, S. Borri, G. Scamarcio, B.E. Bernacki, J. Kriesel, Part-per-trillion level SF_6 detection using a quartz enhanced photoacoustic spectroscopy-based sensor with single-mode fiber-coupled quantum cascade laser excitation, Opt. Lett. 37 (2012) 4461, https://doi.org/10.1364/ol.37.004461.
[28] A.A. Kosterev, Y.A. Bakhirkin, F.K. Tittel, Ultrasensitive gas detection by quartz-enhanced photoacoustic spectroscopy in the fundamental molecular absorption bands region, Appl. Phys. B Laser Opt. 80 (2005) 133–138, https://doi.org/10.1007/s00340-004-1619-y.
[29] S. Dello Russo, A. Sampaolo, P. Patimisco, G. Menduni, M. Giglio, C. Hoelzl, V.M.N. Passaro, H. Wu, L. Dong, V. Spagnolo, Photoacoustics Quartz-enhanced photoacoustic spectroscopy exploiting low-frequency tuning forks as a tool to measure the vibrational relaxation rate in gas species, Photoacoustics 21 (2021), 100227, https://doi.org/10.1016/j.pacs.2020.100227.
[30] P. Repond, M.W. Sigrist, Photoacoustic spectroscopy on trace gases with continuously tunable CO_2 laser, Appl. Opt. 35 (1996) 4065, https://doi.org/10.1364/ao.35.004065.
[31] G. Wysocki, A.A. Kosterev, F.K. Tittel, Influence of molecular relaxation dynamics on quartz-enhanced photoacoustic detection of CO_2 at $\lambda = 2$ μm, Appl. Phys. B Laser Opt. 85 (2006) 301–306, https://doi.org/10.1007/s00340-006-2369-9.
[32] A. Sampaolo, C. Yu, T. Wei, A. Zifarelli, M. Giglio, H_2S quartz-enhanced photoacoustic spectroscopy sensor employing a liquid-nitrogen-cooled THz quantum cascade laser operating in pulsed mode, Photoacoustics 21 (2021), https://doi.org/10.1016/j.pacs.2020.100219.
[33] P. Patimisco, S. Borri, A. Sampaolo, H.E. Beere, D.A. Ritchie, M.S. Vitiello, G. Scamarcio, V. Spagnolo, A quartz enhanced photo-acoustic gas sensor based on a custom tuning fork and a terahertz quantum cascade laser, Analyst 139 (2014) 2079–2087, https://doi.org/10.1039/c3an01219k.
[34] A. Sampaolo, P. Patimisco, M. Giglio, M.S. Vitiello, H.E. Beere, D.A. Ritchie, G. Scamarcio, F.K. Tittel, V. Spagnolo, Improved tuning fork for terahertz quartz-enhanced photoacoustic spectroscopy, Sensors 16 (2016), https://doi.org/10.3390/s16040439.
[35] A. Sampaolo, P. Patimisco, L. Dong, A. Geras, G. Scamarcio, T. Starecki, F.K. Tittel, V. Spagnolo, Quartz-enhanced photoacoustic spectroscopy exploiting tuning fork overtone modes, Appl. Phys. Lett. 107 (2015), https://doi.org/10.1063/1.4937002.
[36] F.K. Tittel, A. Sampaolo, P. Patimisco, L. Dong, A. Geras, T. Starecki, V. Spagnolo, Analysis of overtone flexural modes operation in quartz-enhanced photoacoustic spectroscopy, Opt Express 24 (2016), https://doi.org/10.1364/OE.24.00A682.
[37] H. Zheng, L. Dong, P. Patimisco, H. Wu, A. Sampaolo, X. Yin, S. Li, W. Ma, L. Zhang, W. Yin, L. Xiao, V. Spagnolo, S. Jia, F.K. Tittel, Double antinode excited quartz-enhanced photoacoustic spectrophone, Appl. Phys. Lett. 110 (2017), https://doi.org/10.1063/1.4973858.
[38] H. Wu, X. Yin, L. Dong, K. Pei, A. Sampaolo, P. Patimisco, H. Zheng, W. Ma, L. Zhang, W. Yin, L. Xiao, V. Spagnolo, S. Jia, F.K. Tittel, Simultaneous dual-gas QEPAS detection based on a fundamental and overtone combined vibration of quartz tuning fork, Appl. Phys. Lett. 110 (2017), https://doi.org/10.1063/1.4979085.
[39] M. Giglio, A. Elefante, P. Patimisco, A. Sampaolo, F. Sgobba, H. Rossmadl, V. Mackowiak, H. Wu, F.K. Tittel, L. Dong, V. Spagnolo, Quartz-enhanced photoacoustic sensor for ethylene detection implementing optimized custom tuning fork-based spectrophone, Opt Express 27 (2019) 4271, https://doi.org/10.1364/oe.27.004271.
[40] S. Li, L. Dong, H. Wu, A. Sampaolo, P. Patimisco, V. Spagnolo, F.K. Tittel, Ppb-level quartz-enhanced photoacoustic detection of carbon monoxide exploiting a surface grooved tuning fork, Anal. Chem. 91 (2019) 5834–5840, https://doi.org/10.1021/acs.analchem.9b00182.
[41] B. Sun, A. Zifarelli, H. Wu, S. Dello Russo, S. Li, P. Patimisco, L. Dong, V. Spagnolo, Mid-infrared quartz-enhanced photoacoustic sensor for ppb-level CO detection in a SF_6Gas matrix exploiting a T-Grooved quartz tuning fork, Anal. Chem. 92 (2020) 13922–13929, https://doi.org/10.1021/acs.analchem.0c02772.
[42] H. Hosaka, K. Itao, S. Kuroda, Damping characteristics of beam-shaped micro-oscillators, Sensors Actuators, A Phys. 49 (1995) 87–95, https://doi.org/10.1016/0924-4247(95)01003-J.
[43] Z. Hao, A. Erbil, F. Ayazi, An analytical model for support loss in micromachined beam resonators with in-plane flexural vibrations, Sensors Actuators, A Phys. 109 (2003) 156–164, https://doi.org/10.1016/j.sna.2003.09.037.
[44] P. Patimisco, A. Sampaolo, V. Mackowiak, H. Rossmadl, A. Cable, F.K. Tittel, V. Spagnolo, Loss mechanisms determining the quality factors in quartz tuning forks vibrating at the fundamental and first overtone modes, IEEE Trans. Ultrason. Ferroelectrics Freq. Contr. 65 (2018) 1951–1957, https://doi.org/10.1109/TUFFC.2018.2853404.
[45] S. Qiao, Y. Ma, P. Patimisco, A. Sampaolo, Y. He, Z. Lang, F.K. Tittel, V. Spagnolo, Multi-pass quartz-enhanced photoacoustic spectroscopy-based trace gas sensing, Opt. Lett. 46 (2021) 977, https://doi.org/10.1364/ol.418520.
[46] Y. Ma, S. Qiao, P. Patimisco, A. Sampaolo, Y. Wang, F.K. Tittel, V. Spagnolo, In-plane quartz-enhanced photoacoustic spectroscopy, Appl. Phys. Lett. 116 (2020), https://doi.org/10.1063/1.5142330.
[47] S. Dello Russo, M. Giglio, A. Sampaolo, P. Patimisco, G. Menduni, H. Wu, L. Dong, V.M.N. Passaro, V. Spagnolo, Acoustic coupling between resonator tubes in quartz-enhanced photoacoustic spectrophones employing a large prong spacing tuning fork, Sensors 19 (2019), https://doi.org/10.3390/s19194109.
[48] H. Wu, A. Sampaolo, L. Dong, P. Patimisco, X. Liu, H. Zheng, X. Yin, W. Ma, L. Zhang, W. Yin, V. Spagnolo, S. Jia, F.K. Tittel, Quartz enhanced photoacoustic H2S gas sensor based on a fiber-amplifier source and a custom tuning fork with large prong spacing, Appl. Phys. Lett. 107 (2015) 2–7, https://doi.org/10.1063/1.4930995.
[49] M. Giglio, P. Patimisco, A. Sampaolo, A. Zifarelli, R. Blanchard, C. Pfluegl, M.F. Witinski, D. Vakhshoori, F.K. Tittel, V. Spagnolo, Nitrous oxide quartz-enhanced photoacoustic detection employing a broadband distributed-feedback quantum cascade laser array, Appl. Phys. Lett. 113 (2018) 1–5, https://doi.org/10.1063/1.5049872.
[50] H. Zheng, L. Dong, A. Sampaolo, H. Wu, P. Patimisco, X. Yin, W. Ma, L. Zhang, W. Yin, V. Spagnolo, S. Jia, F.K. Tittel, Single-tube on-beam quartz-enhanced photoacoustic spectroscopy, Opt. Lett. 41 (2016) 978, https://doi.org/10.1364/ol.41.000978.
[51] H. Zheng, L. Dong, A. Sampaolo, P. Patimisco, W. Ma, L. Zhang, W. Yin, L. Xiao, V. Spagnolo, S. Jia, F.K. Tittel, Overtone resonance enhanced single-tube on-beam quartz enhanced photoacoustic spectrophone, Appl. Phys. Lett. 109 (2016), https://doi.org/10.1063/1.4962810.
[52] K. Liu, X. Guo, H. Yi, W. Chen, W. Zhang, X. Gao, Off-beam quartz-enhanced photoacoustic spectroscopy, Opt. Lett. 34 (2009) 1594, https://doi.org/10.1364/OL.34.001594.
[53] H. Yi, R. Maamary, X. Gao, M.W. Sigrist, E. Fertein, W. Chen, Short-lived species detection of nitrous acid by external-cavity quantum cascade laser based quartz-enhanced photoacoustic absorption spectroscopy, Appl. Phys. Lett. 106 (2015), https://doi.org/10.1063/1.4914896.
[54] A. Sampaolo, P. Patimisco, M. Giglio, G. Menduni, A. Elefante, V. Passaro, F.K. Tittel, V. Spagnolo, Simultaneous dual gas QEPAS sensing of water and methane/nitrous oxide, in: Proc. SPIE - Int. Soc. Opt. Eng, 2019, https://doi.org/10.1117/12.2507922.
[55] A. Elefante, M. Giglio, A. Sampaolo, G. Menduni, P. Patimisco, V.M.N. Passaro, H. Wu, H. Rossmadl, V. Mackowiak, A. Cable, F.K. Tittel, L. Dong, V. Spagnolo, Dual-gas quartz-enhanced photoacoustic sensor for simultaneous detection of methane/nitrous oxide and water vapor, Anal. Chem. 91 (2019) 12866–12873, https://doi.org/10.1021/acs.analchem.9b02709.
[56] H. Wu, L. Dong, X. Yin, A. Sampaolo, P. Patimisco, W. Ma, L. Zhang, W. Yin, L. Xiao, V. Spagnolo, S. Jia, Atmospheric CH_4 measurement near a landfill using an ICL-based QEPAS sensor with V-T relaxation self-calibration, Sensor. Actuator. B Chem. 297 (2019), 126753, https://doi.org/10.1016/

j.snb.2019.126753.
[57] R. Lewicki, G. Wysocki, A.A. Kosterev, F.K. Tittel, Carbon dioxide and ammonia detection using 2 μm diode laser based quartz-enhanced photoacoustic spectroscopy, Appl. Phys. B Laser Opt. 87 (2007) 157–162, https://doi.org/10.1007/s00340-006-2474-9.
[58] A.A. Kosterev, F.K. Tittel, D.V. Serebryakov, A.L. Malinovsky, I.V. Morozov, Applications of quartz tuning forks in spectroscopic gas sensing, Rev. Sci. Instrum. 76 (2005), https://doi.org/10.1063/1.1884196.
[59] A.A. Kosterev, F.K. Tittel, G. Bearman, Advanced quartz-enhanced photoacoustic trace gas sensor for early fire detection, SAE Int. J. Aerosp 1 (2009) 331–336, https://doi.org/10.4271/2008-01-2091.
[60] L. Dong, J. Wright, B. Peters, B.A. Ferguson, F.K. Tittel, S. McWhorter, Compact QEPAS sensor for trace methane and ammonia detection in impure hydrogen, Appl. Phys. B Laser Opt. 107 (2012) 459–467, https://doi.org/10.1007/s00340-012-4908-x.
[61] L. Dong, A.A. Kosterev, D. Thomazy, F.K. Tittel, Compact portable QEPAS multi-gas sensor, Quantum Sens. Nanophotonic Devices VIII 7945 (2011) 79450R, https://doi.org/10.1117/12.875108.
[62] I.E. Gordon, L.S. Rothman, C. Hill, R.V. Kochanov, Y. Tan, P.F. Bernath, M. Birk, V. Boudon, A. Campargue, K.V. Chance, B.J. Drouin, J.M. Flaud, R.R. Gamache, J.T. Hodges, D. Jacquemart, V.I. Perevalov, A. Perrin, K.P. Shine, M.A.H. Smith, J. Tennyson, G.C. Toon, H. Tran, V.G. Tyuterev, A. Barbe, A.G. Császár, V.M. Devi, T. Furtenbacher, J.J. Harrison, J.M. Hartmann, A. Jolly, T.J. Johnson, T. Karman, I. Kleiner, A.A. Kyuberis, J. Loos, O.M. Lyulin, S.T. Massie, S.N. Mikhailenko, N. Moazzen-Ahmadi, H.S.P. Müller, O.V. Naumenko, A.V. Nikitin, O.L. Polyansky, M. Rey, M. Rotger, S.W. Sharpe, K. Sung, E. Starikova, S.A. Tashkun, J. Vander Auwera, G. Wagner, J. Wilzewski, P. Wcisło, S. Yu, E.J. Zak, The HITRAN2016 molecular spectroscopic database,, J. Quant. Spectrosc. Radiat. Transf. 203 (2017) 3–69, https://doi.org/10.1016/j.jqsrt.2017.06.038.
[63] F. Merkt, M. Quack, Molecular Quantum Mechanics and Molecular Spectra, Molecular Symmetry, and Interaction of Matter with Radiation, 2011, https://doi.org/10.1002/9780470749593.hrs001.
[64] S.G. Jennings, Atmospheric trace gases and aerosols, Remote Sens. Glob. Clim. Chang 124 (1994) 223–252, https://doi.org/10.1007/978-3-642-79287-8_10.
[65] Y. Ma, R. Lewicki, M. Razeghi, F.K. Tittel, QEPAS based ppb-level detection of CO and N_2O using a high power CW DFB-QCL, Opt Express 21 (2013) 1008, https://doi.org/10.1364/oe.21.001008.
[66] M. Giglio, P. Patimisco, A. Sampaolo, G. Scamarcio, F.K. Tittel, V. Spagnolo, Allan deviation plot as a tool for quartz-enhanced photoacoustic sensors noise analysis, IEEE Trans. Ultrason. Ferroelectrics Freq. Contr. 63 (2016) 555–560, https://doi.org/10.1109/TUFFC.2015.2495013.
[67] M. Jahjah, W. Jiang, N.P. Sanchez, W. Ren, P. Patimisco, V. Spagnolo, S.C. Herndon, R.J. Griffin, F.K. Tittel, Atmospheric CH_4 and N_2O measurements near Greater Houston area landfills using a QCL-based QEPAS sensor system during DISCOVER-AQ 2013, Opt. Lett. 39 (2014) 957, https://doi.org/10.1364/ol.39.000957.
[68] Y. Cao, N.P. Sanchez, W. Jiang, R.J. Griffin, F. Xie, L.C. Hughes, C. Zah, F.K. Tittel, Simultaneous atmospheric nitrous oxide, methane and water vapor detection with a single continuous wave quantum cascade laser, Opt Express 23 (2015) 2121, https://doi.org/10.1364/oe.23.002121.
[69] A. Sampaolo, G. Menduni, P. Patimisco, M. Giglio, V.M.N. Passaro, L. Dong, H. Wu, F.K. Tittel, V. Spagnolo, Quartz-enhanced photoacoustic spectroscopy for hydrocarbon trace gas detection and petroleum exploration, Fuel 277 (2020) 1–26, https://doi.org/10.1016/j.fuel.2020.118118.
[70] V. Spagnolo, L. Dong, A.A. Kosterev, F.K. Tittel, Modulation cancellation method for isotope 18O/16O ratio measurements in water, Opt Express 20 (2012) 3401, https://doi.org/10.1364/oe.20.003401.
[71] Z. Wang, Q. Wang, J.Y.L. Ching, J.C.Y. Wu, G. Zhang, W. Ren, A portable low-power QEPAS-based CO_2 isotope sensor using a fiber-coupled interband cascade laser, Sensor. Actuator. B Chem. 246 (2017) 710–715, https://doi.org/10.1016/j.snb.2017.02.133.
[72] F. Musat, C. Vogt, H.H. Richnow, Carbon and hydrogen stable isotope fractionation associated with the aerobic and anaerobic degradation of saturated and alkylated aromatic hydrocarbons, J. Mol. Microbiol. Biotechnol. 26 (2016) 211–226, https://doi.org/10.1159/000442161.
[73] V. Spagnolo, L. Dong, A.A. Kosterev, D. Thomazy, J.H. Doty, F.K. Tittel, Modulation cancellation method in laser spectroscopy, Appl. Phys. B Laser Opt. 103 (2011) 735–742, https://doi.org/10.1007/s00340-011-4494-3.
[74] V. Spagnolo, L. Dong, A.A. Kosterev, D. Thomazy, J.H. Doty III, F.K. Tittel, Modulation cancellation method for measurements of small temperature differences in a gas, Opt. Lett. 36 (2011) 460, https://doi.org/10.1364/ol.36.000460.
[75] A.A. Kosterev, Y.A. Bakhirkin, F.K. Tittel, S. Blaser, Y. Bonetti, L. Hvozdara, Photoacoustic phase shift as a chemically selective spectroscopic parameter, Appl. Phys. B Laser Opt. 78 (2004) 673–676, https://doi.org/10.1007/s00340-004-1519-1.
[76] R.A. Rooth, A.J.L. Verhage, L.W. Wouters, Photoacoustic measurement of ammonia in the atmosphere: influence of water vapor and carbon dioxide, Appl. Opt. 29 (1990) 3643, https://doi.org/10.1364/ao.29.003643.
[77] E. Avramides, T.F. Hunter, Vibrational-vibrational and vibrational-translational/rotational processes in methane, oxygen gas-phase mixtures optoacoustic measurements, Mol. Phys. 48 (1983) 1331–1343, https://doi.org/10.1080/00268978300100951.
[78] Z. Wang, J. Geng, W. Ren, Quartz-enhanced photoacoustic spectroscopy (QEPAS) detection of the ν7 band of ethylene at low pressure with CO_2 interference analysis, Appl. Spectrosc. 71 (2017) 1834–1841, https://doi.org/10.1177/0003702817690406.
[79] M.S. Bartlett, Multivariate analysis, Suppl. to J. R. Stat. Soc 9 (1947) 176, https://doi.org/10.2307/2984113.
[80] S. Wold, A. Ruhe, H. Wold, W.J. Dunn III, The collinearity problem in linear regression. The partial least squares (PLS) approach to generalized inverses, SIAM J. Sci. Stat. Comput. 5 (1984) 735–743, https://doi.org/10.1137/0905052.
[81] D.M. Hawkins, The problem of overfitting, J. Chem. Inf. Comput. Sci. 44 (2004) 1–12, https://doi.org/10.1021/ci0342472.
[82] A. Sampaolo, S. Csutak, P. Patimisco, M. Giglio, G. Menduni, V. Passaro, F.K. Tittel, M. Deffenbaugh, V. Spagnolo, Methane, ethane and propane detection using a compact quartz enhanced photoacoustic sensor and a single interband cascade laser, Sensors Actuators, Biol. Chem. 282 (2019) 952–960, https://doi.org/10.1016/j.snb.2018.11.132.
[83] M. Giglio, A. Zifarelli, A. Sampaolo, G. Menduni, A. Elefante, R. Blanchard, C. Pfluegl, M.F. Witinski, D. Vakhshoori, H. Wu, V.M.N. Passaro, P. Patimisco, F.K. Tittel, L. Dong, V. Spagnolo, Broadband detection of methane and nitrous oxide using a distributed-feedback quantum cascade laser array and quartz-enhanced photoacoustic sensing, Photoacoustics 17 (2020), 100159, https://doi.org/10.1016/j.pacs.2019.100159.
[84] G. Menduni, F. Sgobba, S. Dello Russo, A.C. Ranieri, A. Sampaolo, P. Patimisco, M. Giglio, V.M.N. Passaro, S. Csutak, D. Assante, E. Ranieri, E. Geoffrion, V. Spagnolo, Fiber-coupled quartz-enhanced photoacoustic spectroscopy system for methane and ethane monitoring in the near-infrared spectral range, Molecules 25 (2020) 5607, https://doi.org/10.3390/molecules25235607.
[85] L.G. Smith, The infra-red spectrum of C_2H_6, J. Chem. Phys. 17 (1949) 139–167, https://doi.org/10.1063/1.1747206.
[86] X. Tian, Y. Cao, J. Chen, K. Liu, G. Wang, T. Tan, J. Mei, W. Chen, X. Gao, Dual-gas sensor of CH_4/C_2H_6 based on wavelength modulation spectroscopy coupled to a home-made compact dense-pattern multipass cell, Sensors 19 (2019), https://doi.org/10.3390/s19040820.
[87] F. Sgobba, G. Menduni, S. Dello Russo, A. Sampaolo, P. Patimisco, M. Giglio, E. Ranieri, V.M.N. Passaro, F.K. Tittel, V. Spagnolo, Quartz-enhanced photoacoustic detection of ethane in the near-IR exploiting a highly performant spectrophone, Appl. Sci. 10 (2020) 1–11, https://doi.org/10.3390/app10072447.
[88] M. Hepp, M. Herman, Vibration-rotation bands in ethane, Mol. Phys. 98 (2000) 57–61, https://doi.org/10.1080/00268970009483269.
[89] H. Bruhns, M. Wolff, Y. Saalberg, K.M. Spohr, Quantitative evaluation of broadband photoacoustic spectroscopy in the infrared with an optical parametric oscillator, Sensors 18 (2018) 1–16, https://doi.org/10.3390/s18113971.
[90] K. Kafadar, S. Kotz, C. Read, D. Banks, Encyclopedia of statistical sciences, J. Am. Stat. Assoc. 92 (1997) 1653, https://doi.org/10.2307/2965452.
[91] S. Wold, M. Sjöström, L. Eriksson, PLS-regression: a basic tool of chemometrics, Chemometr. Intell. Lab. Syst. 58 (2001) 109–130, https://doi.org/10.1016/S0169-7439(01)00155-1.
[92] K. Wongravee, N. Heinrich, M. Holmboe, M.L. Schaefer, R.R. Reed, J. Trevejo, R.G. Brereton, Variable selection using iterative reformulation of training set models for discrimination of samples: application to gas chromatography/mass spectrometry of mouse urinary metabolites, Anal. Chem. 81 (2009) 5204–5217, https://doi.org/10.1021/ac900251c.
[93] A. Zifarelli, M. Giglio, G. Menduni, A. Sampaolo, P. Patimisco, V.M.N Passaro, H. Wu, L. Dong, V. Spagnolo, Partial Least Squares Regression as a Tool to Retrieve Gas Concentrations in Mixtures Detected by Using Quartz-Enhanced Photoacoustic Spectroscopy (2020), https://doi.org/10.1021/acs.analchem.0c00075.
[94] R. Lewicki, G. Wysocki, A.A. Kosterev, F.K. Tittel, QEPAS based detection of broadband absorbing molecules using a widely tunable, cw quantum cascade laser at 8.4 μm, Opt Express 15 (2007) 7357, https://doi.org/10.1364/oe.15.007357.
[95] A.A. Kosterev, P.R. Buerki, L. Dong, M. Reed, T. Day, F.K. Tittel, QEPAS detector for rapid spectral measurements, Appl. Phys. B Laser Opt. 100 (2010) 173–180, https://doi.org/10.1007/s00340-010-3975-0.
[96] L. Dong, A.A. Kosterev, D. Thomazy, F.K. Tittel, QEPAS spectrophones: design, optimization, and performance, Appl. Phys. B Laser Opt. 100 (2010) 627–635, https://doi.org/10.1007/s00340-010-4072-0.
[97] C. Gutt, B. Asmussen, W. Press, M.R. Johnson, Y.P. Handa, J.S. Tse, The structure of deuterated methane–hydrate, J. Chem. Phys. 113 (2000) 4713–4721, https://doi.org/10.1063/1.1288789.
[98] A. Bajtarevic, C. Ager, M. Pienz, M. Klieber, K. Schwarz, M. Ligor, T. Ligor, W. Filipiak, H. Denz, M. Fiegl, W. Hilbe, W. Weiss, P. Lukas, H. Jamnig, M. Hackl, A. Haidenberger, B. Buszewski, W. Miekisch, J. Schubert, A. Amann, Noninvasive detection of lung cancer by analysis of exhaled breath, BMC Canc. 9 (2009) 348, https://doi.org/10.1186/1471-2407-9-348.
[99] C. Wang, P. Sahay, Breath analysis using laser spectroscopic techniques: breath biomarkers, spectral fingerprints, and detection limits, Sensors 9 (2009) 8230–8262, https://doi.org/10.3390/s91008230.
[100] J. Wojtas, F.K. Tittel, T. Stacewicz, Z. Bielecki, R. Lewicki, J. Mikolajczyk, M. Nowakowski, D. Szabra, P. Stefanski, J. Tarka, Cavity-enhanced absorption spectroscopy and photoacoustic spectroscopy for human breath analysis, Int. J. Thermophys. 35 (2014) 2215–2225, https://doi.org/10.1007/s10765-014-

1586-4.
[101] A.A. Kosterev, L. Dong, D. Thomazy, F.K. Tittel, S. Overby, QEPAS for chemical analysis of multi-component gas mixtures, Appl. Phys. B Laser Opt. 101 (2010) 649–659, https://doi.org/10.1007/s00340-010-4183-7.
[102] G. Menduni, A. Sampaolo, S. Csutak, P. Patimisco, M. Giglio, A. Elefante, V. Passaro, F.K. Tittel, M. Deffenbaugh, V. Spagnolo, Quartz-enhanced Photoacoustic Sensors for Detection of Multiple Hydrocarbon and Methane Isotopes, vol. 11, 2019, https://doi.org/10.1117/12.2507881.
[103] T. Takahashi, B. Thornton, Quantitative methods for compensation of matrix effects and self-absorption in LIBS signals of solids, Spectrochim. Acta Part B At. Spectrosc 138 (2017) 31–42, https://doi.org/10.1016/j.sab.2017.09.010.
[104] Z.Q. Hao, C.M. Li, M. Shen, X.Y. Yang, K.H. Li, L.B. Guo, X.Y. Li, Y.F. Lu, X.Y. Zeng, Acidity measurement of iron ore powders using laser-induced breakdown spectroscopy with partial least squares regression, Opt Express 23 (2015) 7795, https://doi.org/10.1364/oe.23.007795.
[105] M. Mordmueller, W. Schade, U. Willer, QEPAS with electrical co-excitation for photoacoustic measurements in fluctuating background gases, Appl. Phys. B Laser Opt. 123 (2017) 1–9, https://doi.org/10.1007/s00340-017-6799-3.
[106] M. Mordmueller, S. Edelmann, M. Knestel, W. Schade, U. Willer, Phase optimized photoacoustic sensing of gas mixtures, Appl. Sci. 10 (2020), https://doi.org/10.3390/app10020438.
[107] H. Wu, L. Dong, H. Zheng, Y. Yu, W. Ma, L. Zhang, W. Yin, L. Xiao, S. Jia, F.K. Tittel, Beat frequency quartz-enhanced photoacoustic spectroscopy for fast and calibration-free continuous trace-gas monitoring, Nat. Commun. 8 (2017) 1–8, https://doi.org/10.1038/ncomms15331.
[108] R. Rousseau, N. Maurin, W. Trzpil, M. Bahriz, A. Vicet, Quartz tuning fork resonance tracking and application in quartz enhanced photoacoustics spectroscopy, Sensors 19 (2019) 5565, https://doi.org/10.3390/s19245565.
[109] R. Levy, M. Duquesnoy, J.-M. Melkonian, M. Raybaut, G. Aoust, New signal processing for fast and precise QEPAS measurements, IEEE Trans. Ultrason. Ferroelectrics Freq. Contr. 67 (2020) 1230–1235, https://doi.org/10.1109/TUFFC.2019.2943388.
[110] X. Yin, L. Dong, H. Zheng, X. Liu, H. Wu, Y. Yang, W. Ma, L. Zhang, W. Yin, L. Xiao, S. Jia, Impact of humidity on quartz-enhanced photoacoustic spectroscopy based CO detection using a near-IR telecommunication diode laser, Sensors 16 (2016), https://doi.org/10.3390/s16020162.
[111] C. Chen, Q. Ren, Y.Z. Wang, Review on multi gas detector using infrared spectral absorption technology, Appl. Spectrosc. Rev. 54 (2019) 425–444, https://doi.org/10.1080/05704928.2018.1474766.
[112] J.C. Petersen, L. Lamard, Y. Feng, J.-F. Focant, A. Peremans, M. Lassen, Quartz-enhanced photo-acoustic spectroscopy for breath analyses, Opt. Biophotonics Low-Resource Settings III. 10055 (2017), 1005503, https://doi.org/10.1117/12.2252896.
[113] C. Gaudiuso, A. Volpe, A. Ancona, One-step femtosecond laser stealth dicing of quartz, Micromachines 11 (2020) 1–11, https://doi.org/10.3390/mi11030327.
[114] M. De Carlo, G. Menduni, A. Sampaolo, F. De Leonardis, V. Spagnolo, V.M.N. Passaro, Modeling and design of a semi-integrated QEPAS sensor, J. Lightwave Technol. 39 (2020), 1–1, https://doi.org/10.1109/jlt.2020.3030682.

Angelo Sampaolo obtained his Master degree in Physics in 2013 and the PhD Degree in Physics in 2017 from University of Bari. He was a visiting researcher in the Laser Science Group at Rice University from 2014 to 2016. Since March 2021, he is a assistant professor at the Technical University of Bari. His research activity has included the study of the thermal properties of heterostructured devices via Raman spectroscopy. Most recently, his research interest has focused on the development of innovative techniques in trace gas sensing, based on Quartz-Enhanced Photoacoustic Spectroscopy and covering the full spectral range from near-IR to THz. His achieved results have been acknowledged by a cover paper in Applied Physics Letter of the July 2013 issue.

Pietro Patimisco obtained the Master degree in Physics (cum laude) in 2009 and the PhD Degree in Physics in 2013 from the University of Bari. Since 2020, he is Assistant professor at the University of Bari. He was a visiting scientist in the Laser Science Group at Rice University in 2013 and 2014. Dr. Patimisco's scientific activity addressed both micro-probe optical characterization of semiconductor optoelectronic devices and optoacoustic gas sensors. Recently, his research activities included the study and applications of trace-gas sensors, such as quartz enhanced photoacoustic spectroscopy and cavity enhanced absorption spectroscopy in the mid infrared and terahertz spectral region, leading to several publications, including a cover paper in Applied Physics Letter of the July 2013 issue.

Marilena Giglio received the M.S. degree (cum laude) in Applied Physics in 2014, and the PhD Degree in Physics in 2018 from the University of Bari. In 2012 she's been visiting the Academic Medical Center of Amsterdam as a trainee. In 2015 she was a Research Assistant with the Department of Physics, University of Bari. She was a visiting researcher in the Laser Science Group at Rice University from 2016 to 2017. Since 2020, she is Assistant Professor at the Technical University of Bari. Her research activity is focused on the development of gas sensors based on Quartz-Enhanced Photoacoustic Spectroscopy and on the optical coupling of hollow-core waveguides with interband- and quantum-cascade lasers.

Andrea Zifarelli obtained his M.S. degree (cum laude) in Physics in 2018 from the University of Bari. From the same year, he is a PhD student at the Physics Department of the University of Bari, developing his research work at PolySense Lab, joint-research laboratory between Technical University of Bari and THORLABS GmbH. Currently, his research activities are focused on the development of gas sensors based on Quartz-Enhanced Photoacoustic Spectroscopy for detection of gas mixtures and broadband absorbers, exploiting non-conventional laser sources.

Hongpeng Wu received his Ph.D. degree in atomic and molecular physics from Shanxi University, China, in 2017. From September 2015 to October 2016, he studied as a joint Ph.D. student in the Electrical and Computer Engineering Department and Rice Quantum Institute, Rice University, Houston, USA. Currently he is a professor in the Institute of Laser Spectroscopy of Shanxi University. His research interests include gas sensors, photoacoustic spectroscopy, photothermal spectroscope and laser spectroscopy techniques.

Lei Dong received his Ph.D. degree in optics from Shanxi University, China, in 2007. From June 2008 to December 2011, he worked as a post-doctoral fellow in the Electrical and Computer Engineering Department and Rice Quantum Institute, Rice University, Houston, USA. Currently he is a professor in the Institute of Laser Spectroscopy of Shanxi University. His research interests include optical sensors, trace gas detection, photoacoustic spectroscopy and laser spectroscopy.

Vincenzo Spagnolo obtained the PhD in physics in 1994 from University of Bari. From 1997 to 1999, he was researcher of the National Institute of the Physics of Matter. Since 2004, he works at the Technical University of Bari, formerly as assistant and associate professor and now as full Professor of Physics. Starting from 2019, he become Vice-Rector of the technical university of Bari - Deputy to Technology Transfer. He is the director of the joint-research lab PolySense between Technical University of Bari and THORLABS GmbH, fellow member of SPIE and senior member of OSA. His research interests include optoacoustic gas sensing and spectroscopic techniques for real-time monitoring. His research activity is documented by more than 220 publications and 3 filed patents. He has given more than 50 invited presentations at international conferences and workshops.